Arteriosclerosis, Thrombosis, and Vascular Biology

BASIC SCIENCES

RNA-Binding Proteins Regulate Post-Transcriptional Responses to TGF-β to Coordinate Function and Mesenchymal Activation of Murine Endothelial Cells

Rhys Wardman, Merve Keles, Ihor Pachkiv, Shruthi Hemanna, Steve Grein, Jennifer Schwarz, Frank Stein, Roxana Ola, Gergana Dobreva, Matthias W. Hentze, Joerg Heineke

BACKGROUND: Endothelial cells (ECs) are primed to respond to various signaling cues. For example, TGF (transforming growth factor)-β has major effects on EC function and phenotype by driving ECs towards a more mesenchymal state (ie, triggering endothelial to mesenchymal activation), a dynamic process associated with cardiovascular diseases. Although transcriptional regulation triggered by TGF-β in ECs is well characterized, post-transcriptional regulatory mechanisms induced by TGF-β remain largely unknown.

METHODS: Using RNA interactome capture, we identified global TGF-β driven changes in RNA-binding proteins in ECs. We investigated specific changes in the RNA-binding patterns of hnRNP H1 (heterogeneous nuclear ribonucleoprotein H1) and Csde1 (cold shock domain containing E1) using RNA immunoprecipitation and overlapped this with RNA-sequencing data after knockdown of either protein for functional insight. Using a modified proximity ligation assay, we visualized the specific interactions between hnRNP H1 and Csde1 and target RNAs in situ both in vitro and in mouse heart sections.

RESULTS: Characterization of TGF-β–regulated RBPs (RNA-binding proteins) revealed hnRNP H1 and Csde1 as key regulators of the cellular response to TGF-β at the post-transcriptional level, with loss of either protein-promoting mesenchymal activation in ECs. We found that TGF-β drives an increase in binding of hnRNP H1 to its target RNAs, offsetting mesenchymal activation, but a decrease in Csde1 RNA-binding, facilitating this process. Both, hnRNP H1 and Csde1, dynamically bind and regulate specific subsets of mRNAs related to mesenchymal activation and endothelial function.

CONCLUSIONS: Together, we show that RBPs play a key role in the endothelial response to TGF-β stimulation at the post-transcriptional level and that the RBPs hnRNP H1 and Csde1 serve to maintain EC function and counteract mesenchymal activation. We propose that TGF-β profoundly modifies RNA-protein interaction entailing feedback and feed-forward control at the post-transcriptional level, to fine-tune mesenchymal activation in ECs.

GRAPHIC ABSTRACT: A graphic abstract is available for this article.

Key Words: endothelial cells ■ heterogeneous nuclear ribonucleoprotein ■ phenotype ■ RNA-binding proteins ■ transforming growth factors

Endothelial cells (ECs) constitute the inner layer of all blood vessels. In the microvasculature, capillary ECs form a vast network serving not only to deliver nutrients and oxygen but also to regulate, for instance, tissue perfusion, blood coagulation, and the trafficking of inflammatory cells. Given their position, these ECs

Correspondence to: Rhys Wardman, PhD, Department of Cardiovascular Physiology, European Center for Angioscience (ECAS), Medical Faculty Mannheim, University of Heidelberg, Ludolf-Krehl-Str. 7-11, 68167 Mannheim, Germany, Email rhys.wardman@medma.uni-heidelberg.de; or Joerg Heineke, MD, Department of Cardiovascular Physiology, European Center for Angioscience (ECAS), Medical Faculty Mannheim, University of Heidelberg, Ludolf-Krehl-Str. 7-11, 68167 Mannheim, Germany, Email joerg.heineke@medma.uni-heidelberg.de
Supplemental Material is available at https://www.ahajournals.org/doi/suppl/10.1161/ATVBAHA.123.319925.
For Sources of Funding and Disclosures, see page 1988.

Arterioscler Thromb Vasc Biol is available at www.ahajournals.org/journal/atvb

Nonstandard Abbreviations and Acronyms

bFGF	basic fibroblast growth factor
Csde1	cold shock domain containing E1
EC	endothelial cells
EGF	epidermal growth factor
EndoMA	endothelial to mesenchymal activation
HCMEC	human cardiac microvascular endothelial cells
hnRNP H1	heterogeneous nuclear ribonucleoprotein H1
HUVEC	human umbilical vein endothelial cells
MCECs	mouse cardiac endothelial cells
mTOR	mammalian target of rapamycin
PLA	proximity ligation assay
qPCR	quantitative polymerase chain reaction
RBP	RNA-binding protein
RIC	RNA interactome capture
RIP	RNA immunoprecipitation
RIP-seq	RNA immunoprecipitation sequencing
RNA-seq	RNA-sequencing
TAC	transverse aortic constriction
TGF	transforming growth factor
UTR	untranslated region

Highlights

- TGF (transforming growth factor)-β stimulation results in widespread changes in binding of RBPs (RNA-binding proteins) to RNA.
- Changes in the RNA-binding patterns of several key RBPs closely correlate with the activation of a more mesenchymal phenotype in endothelial cells.
- TGF-β stimulation results in opposing changes in the proportion of RNA-bound hnRNP H1 (heterogeneous nuclear ribonucleoprotein H1) and Csde1 (cold shock domain containing E1), although both proteins are protective in maintaining endothelial cell function and offsetting endothelial to mesenchymal activation.
- TGF-β results in a distinct increase in the affinity of hnRNP H1 to specific subsets of RNAs involved in endothelial function and mesenchymal characteristics, decreasing the expression of mesenchymal RNAs, and offsetting endothelial to mesenchymal activation.
- TGF-β results in decreased affinity for Csde1 to mesenchymal-related RNAs, thereby facilitating their increased expression and promoting mesenchymal activation.

are primed to receive signaling cues from their microenvironment, for example, through growth factor stimulation both under physiological conditions like during development but also during disease.[1,2] As a reaction to stimulation by various growth factors, ECs mediate wide-ranging responses such as increased angiogenesis to form new vessels, release instructive cues to other cells, or undergo phenotypic changes such as the adoption of more mesenchymal-like characteristics.

The capacity of ECs to become more mesenchymal, beginning with endothelial to mesenchymal activation (EndoMA) and culminating under certain conditions in selected organs in full endothelial to mesenchymal transition, is highly dynamic and context-dependent and involves, to varying extents, reduced endothelial and increased mesenchymal gene expression accompanied with changed phenotypic traits resulting in a loss of endothelial characteristics and a gain of a more mesenchymal-like phenotype.[3,4] Although endothelial to mesenchymal transition is essential for cardiac development, including valve formation, septa formation, and endocardial differentiation, recent evidence implicates mesenchymal activation of ECs in a range of postnatal cardiovascular pathologies such as myocardial fibrosis during myocardial infarction or cardiac pressure overload, atherosclerosis, and valvular disease.[5–9]

TGF (transforming growth factor)-β plays key roles in development, tissue differentiation, homeostasis, and repair that is known to exert a range of effects on the endothelium and is assigned to be the master driver in the activation of ECs towards a more mesenchymal state.[3,4,10,11] The mechanisms of TGF-β signaling at the transcriptional level, that is, activation of TGF-β receptor type I and II complexes at the plasma membrane resulting in activation of SMAD (suppressor of mothers against decapentaplegic) transcription factors and subsequent changes in gene expression, have been extensively studied.[11–13] However, the response of ECs to TGF-β stimulation at the post-transcriptional level, and the role of the post-transcriptional responses in coordinating changes in the endothelial phenotype, remain to be investigated.

RBPs (RNA-binding proteins) regulate all aspects of RNA metabolism, including transcript localization, splicing, stability, nuclear export as well as translational efficiency. Therefore, RBPs are key regulators of gene expression at the post-transcriptional level. As RNA-protein interactions are highly dynamic, changes in RNA-binding activity serve as a primary reaction to environmental cues such as intercellular paracrine signaling, entailing specific changes of the proteome to orchestrate the cellular response.[14,15] Although many RBPs are known to play important roles in endothelial function and dysfunction, for instance, HuR (human antigen R), which promotes inflammatory activation by stabilizing mRNA of proinflammatory genes, the extent of the contribution of RBPs in ECs remains to be fully elucidated.[16,17]

The development of techniques such as RNA interactome capture (RIC) allow the comparative analysis of

global changes in RNA-binding patterns between different (patho-) physiological conditions, providing invaluable insight into the role of RNA-protein interactions during health and disease.[18–20] Utilizing RIC, we identified global changes in RNA-binding patterns of endothelial RBPs on TGF-β exposure. We found that 2 TGF-β–regulated RBPs, hnRNP H1 (heterogeneous nuclear ribonucleoprotein H1), and Csde1 (cold shock domain containing E1), bind dynamically to RNA in contrasting manners on TGF-β stimulation.

Intriguingly, we show that despite TGF-β triggering opposing changes in the proportion of RNA-bound hnRNP H1 and Csde1, both of these proteins protect endothelial characteristics by suppressing TGF-β–mediated mesenchymal activation. Using RNA immunoprecipitation sequencing (RIP-seq) and RNA-sequencing (RNA-seq), we identified the specific and functionally relevant RNAs to which both hnRNP H1 and Csde1 bind and characterized interactions both in vitro and in vivo in mouse cardiac tissue. Ultimately, we demonstrate that RBPs play a central role in the response of ECs to TGF-β at the post-transcriptional level and that 2 canonical RBPs, hnRNP H1 and Csde1, might serve as future therapeutic targets to counteract endothelial mesenchymal activation during disease.

MATERIALS AND METHODS

Data Availability

The data that support the findings of this study are available from the corresponding author on reasonable request. Furthermore, RIC, RIP-seq, and RNA-seq data can be found in the Supplemental Material of this article. Raw and processed data for RIP-seq and RNA-sequencing libraries have been deposited to the GEO (Gene Expression Omnibus) repository (reference sequence GSE216228).

Experimental Models

Mice

Male C57Bl6N mice (Charles River Laboratories) aged 8 to 10 weeks were used for sham and transverse aortic constriction (TAC) surgery. Animals had access to water and standard diet ad libitum and were maintained on a 12-hour light and dark cycle at room temperature of 22 (±2) °C, humidity 35% to 60%. All animal procedures described in this study were approved by the local state authorities (Regional Council Karlsruhe, 35-9185.81/G-144/18). All procedures including the use and care of animals were performed according to the Guide for the Care and Use of Laboratory Animals published by the National Research Council (National Institutes of Health Publication No. 85-23, revised 1996) and the German animal protection code.

Transverse Aortic Constriction

TAC or sham surgery was performed by subjecting the aorta to a 26-gauge constriction as described previously.[21] Mice were subcutaneously injected with 0.02 mg/kg atropine and 0.1 mg/kg buprenorphine. Anesthesia was induced in an induction chamber with 2% to 3% isoflurane. After oral intubation, mice were connected to a small-animal ventilator (MiniVent Type 845, Harvard Apparatus). Anesthesia was maintained with 2% to 2.5% isoflurane, a left sternal thoracotomy was performed, the thymus was partially removed, and the transverse aorta was tied around a 26 G needle (the same procedure was performed in sham mice, but the ligature was not tied). During surgery, body temperature was maintained at 37 °C with a temperature-controlled heating pad (Föhr Medical Instruments). For organ harvesting, mice were euthanized 2 weeks postsurgery. The heart was immediately removed, washed in chilled PBS followed by 0.5% KCl:PBS, and dissected at the mid-ventricular level. Basal parts of the ventricle were embedded at optimal cutting temperature.

Cell Lines

Mouse cardiac ECs (MCECs) and NIH/3T3 (immortalized fibroblast cell line) cells were cultured according to the manufacturer's instructions. Briefly, cells were cultured in high glucose DMEM (Dulbecco's Modified Eagle Medium; PAN bioscience) containing 5% FCS (fetal calf serum; MCEC) or 10% FCS (NIH/3T3), 1×penicillin-streptomycin, 10 mmol/L HEPES and 1×nonessential amino acids. Cells were cultured under standard conditions (37 °C, 5% CO_2) and used at P5 to P20 for experiments.

Human umbilical vein ECs (HUVECs) and human cardiac microvascular ECs (HCMECs) were cultured according to manufacturer's instructions. In brief, HUVECs were cultured in EC Growth Medium supplemented with growth medium supplement mix (Promocell; containing growth factor cocktail with 0.4% ECGS/H [endothelial cell growth supplement/heparin], 2% FCS, 0.1 ng/mL EGF [epidermal growth factor], 1 µg/mL hydrocortisone, 1 ng/mL bFGF [basic fibroblast growth factor]; Promocell). HCMECs were cultured in EC Growth Medium supplemented with Growth Medium MV supplement mix (Promocell; containing a growth factor cocktail with ECGS/H 0.4%, FCS 5%, EGF 10 ng/mL, hydrocortisone 1 µg/mL). Both HUVECs and HCMECs were used up until passage 5.

HL1 cells were cultured in Claycomb media containing 10% FCS, 0.1 mmol/L norepinephrine, 2 mmol/L L-glutamine, and 1X penicillin-streptomycin.

Method Details

RNA Interactome Capture

RNA interactome capture was performed as published previously (see Castello et al[22] for a detailed experimental procedure) with minor changes. For each biological replicate, 4×10 cm plates of cells were cultured under the conditions indicated in the Figure legend (Figures 1, 2, and 3). Media was removed and cells were washed in chilled PBS. Buffer was aspirated and protein-RNA complexes were cross-linked by ultraviolet irradiation (254 nm, 150 mJ/cm^2). Cells were lysed in 2 mL lysis buffer (500 mM LiCl [lithium chloride], 0.5% [w/v] LiDS [lithium dodecyl sulphate], 5 mM DTT [dithiothreitol], 1 mM EDTA [ethylenediaminetetraacetic acid], 20 mM Tris-HCl pH 7.4, 1× Complete Mini EDTA-free protease inhibitor) and homogenized by passing through a 21 gauge needle and placed on ice.

Two hundred microliters of Oligo $d(T)_{25}$ magnetic bead slurry (NEB [New England Biolabs], S1419S) per sample were removed and equilibrated in lysis buffer. Beads were combined with lysate and incubated for 2 hours at 4 °C. Lysate was separated from beads and placed on ice. Beads were washed

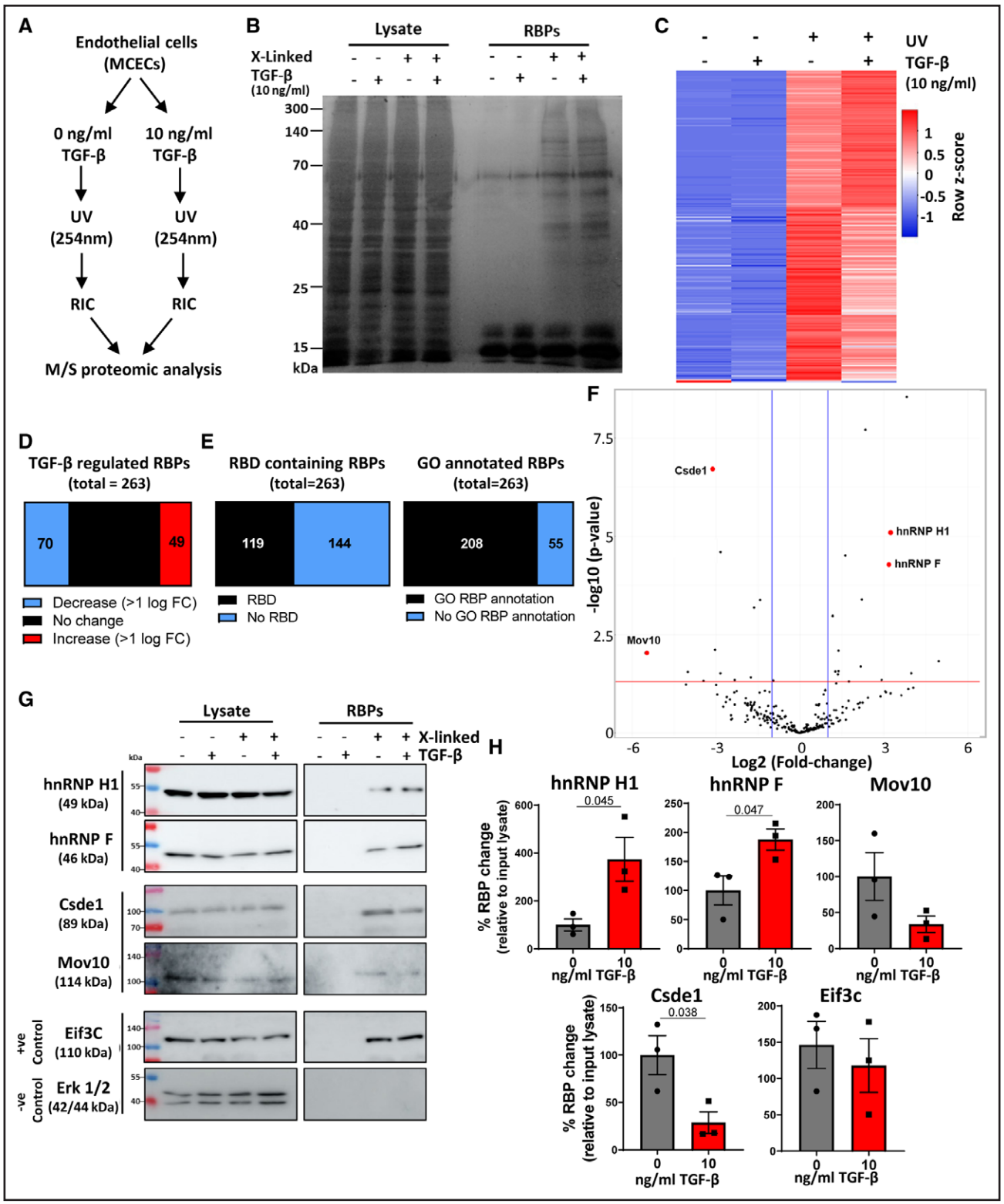

Figure 1. Identification of endothelial TGF (transforming growth factor)-β–regulated RBPs (RNA-binding proteins) using RNA interactome capture.

A, Overview of experimental approach. **B**, Experimental validation. Proteins were isolated by RNA interactome capture (RIC)±ultraviolet (UV) crosslinking and visualized by SDS-PAGE and silver staining. Representative image, n=3. **C**, Heatmap of RBPs. Heatmap of averaged (n=3 independent replicates) abundance of RBPs identified. Columns were ordered by Spearman rank correlation, and rows were colored by *Z* score. **D**, Proportion TGF-β–regulated RBPs. Proportion of TGF-β–regulated RBPs (100% change or greater). **E**, Nonconventional RBPs. RBPs were compared with RBPbase (https://rbpbase.shiny.embl.de/), graphs show proportion of RBPs lacking gene ontology (GO) RBP annotation and canonical RNA-binding domain. **F**, TGF-β–regulated RBPs. Volcano plot showing the fold change (FC; log2) and (*Continued*)

sequentially in lysis buffer, wash buffer I (500 mM LiCl, 0.1% LiDS, 5 mM DTT, 1 mM EDTA, 20 mM Tris-HCl pH 7.4; ×2 washes), wash buffer II (500 mM LiCl, 5 mM DTT, 1 mM EDTA, 20 mM Tris-HCl pH 7.4; ×2 washes), and low salt buffer (200 mM LiCl, 5 mM DTT, 1 mM EDTA, 20 mM Tris-HCl pH 7.4; ×2 washes) each twice for 5 minutes. Samples were briefly centrifuged to remove residual buffer. RNA-protein complexes were eluted in 100 µL elution buffer by heating at 75 °C for 5 minutes, and RNase was digested by addition of 5 µL RNase A/T1 mix for 1 hour at 37 °C.

Mass Spectrometry and Proteomic Analysis

Sample Preparation

Samples from RIC experiments were submitted, processed, and analyzed at the European Molecular Biology Laboratory core proteomics facility, Heidelberg, Germany. Briefly, RIC samples from 3 independent experimental replicates were reduced with DTT (56 °C, 30 minutes, 10 mmol/L in 50 mmol/L HEPES, pH 8.5), followed by alkylation with 2-chloroacetamide (room temperature, in the dark, 30 minutes, 20 mmol/L in 50 mmol/L HEPES, pH 8.5). Samples were subjected to the SP3 (single-pot, solid-phase-enhanced sample-preparation) protocol and peptides were eluted by tryptic digestion (sequencing grade trypsin, Promega) overnight at 37 °C.[23] Peptides were recovered twice in HEPES buffer by collecting the supernatant on a magnet. Both eluates were combined. Peptides were labeled with TMT10plex Isobaric Label Reagent (ThermoFisher) according to the manufacturer's instructions. In short, 0.8 mg reagent was dissolved in 42 µL acetonitrile (100%), and 4 µL of stock was added and incubated for 1 hour at room temperature. The reaction was quenched with 5% hydroxylamine for 15 minutes at room temperature. Samples were combined and desalted using an OASIS HLB µElution Plate (Waters).

Mass Spectrometry

Samples were measured on an Orbitrap Fusion Lumos Tribrid Mass Spectrometer (Thermo) coupled to an UltiMate 3000 RSLC nano LC system (Dionex). Each sample was concentrated on a C18 µ-Precolumn (Acclaim PepMap 100, 5 µm, 300 µm ID ×5 mm, 100 Å) and resolved on a nanoEase M/Z HSS (high-strength silica) T3 column from Waters (75×250 mm C18, 1.8 µm, 100 Å). Trapping was performed at a constant flowrate of 30 µL/min 0.5% trifluoroacetic acid in water for 4 minutes. Subsequently, peptides were eluted via the analytical column (solvent A: 0.1% formic acid in water, 3% dimethyl sulfoxide [DMSO]) with a constant flow of 0.3 µL/min, with increasing percentage of solvent B (0.1% formic acid in acetonitrile, 3% DMSO) from 2% to 8% in 6 minutes, 8% to 28% in 42 minutes, from 28% to 40% in 4 minutes, followed by an increase of solvent B from 40% to 80% for 4 minutes and a reequilibration back to 2% solvent B for 4 minutes.

The peptides were introduced into the Fusion Lumos via a Pico-Tip Emitter 360 µm OD×20 µm ID; 10 µm tip (New Objective) and an applied spray voltage of 2.4 kV. The capillary temperature was at 275 °C. Full mass scan (MS1) was acquired with mass range 375 to 1500 m/z, profile mode, in the orbitrap, resolution of 60 000, fill time 50 ms. Data-dependent acquisition was performed with the resolution of the Orbitrap set to 15 000, fill time 54 ms, AGC target of 1×10^5 ions. Normalized collision energy of 36, HCD, profile mode, fixed first mass 110 m/z.

Data Analysis

IsobarQuant and Mascot (v2.2.07) were used to process the acquired data, which was searched against a Uniprot *Mus musculus* (UP000000589) database containing common contaminants and reversed sequences. The following modifications were considered: carbamidomethyl (C) and TMT10 (K) as fixed modifications, Acetyl (Protein N-term), Oxidation (M), and TMT10 (N-term) as variable modifications. For MS1 (mass spectrometry) spectra, a mass error tolerance of 10 ppm and for MS2 spectra of 0.02 Da was set. Further parameters: trypsin as proteolytic enzyme; maximum 2 missed cleavages; minimum peptide length of 7 amino acids; false discovery rate on peptide; and protein level was set to 0.01.

Following this, raw output files of IsobarQuant were processed using the R programming language. Only proteins that were quantified with at least 2 unique peptides were considered for the analysis (263 proteins passed quality control filtering). Raw signal-sums were cleaned for batch effects using the "removeBatchEffect" function of the limma package and subsequently normalized using variance stabilization normalization. During the normalization, different coefficients were estimated for cross-linked and noncrosslinked conditions to maintain the difference in abundance. Following this, missing values were then imputed with "MinDet" method using the Msnbase package. Differential expression was tested using the limma package. Replicate information was added as a factor in the design matrix given as an argument to the "lmFit" function of limma (imputed values were given a weight of 0.05 in the "lmFit" function). Proteins were annotated as hits with a false discovery rate <5% and a fold change of at least 100% and as a candidate with a false discovery rate below 20% and a fold change of at least 50%.

Silver Staining

RIC and input lysates were mixed with Laemmli sample buffer, boiled, and separated by SDS-PAGE electrophoresis. Gels were fixed in fixation solution (40% ethanol, 10% acetic acid,

Figure 1 Continued. *P* value (–log10) of changes in RIC abundance after TGF-β stimulation. Proteins selected for validation are labeled red. **G**, Validation of selected RBPs. Proteins were isolated by RIC±UV crosslinking and TGF-β stimulation followed by SDS-PAGE and Western blot analysis of selected RBPs from proteomic analysis. Representative images, n=3. **H**, Validation of TGF-β–regulated RBPs. Changes in the abundance of each RNA-binding protein in RIC isolates in the presence of UV-crosslinking (noncrosslinked controls were not quantified as no quantifiable amount of proteins were detected) ±TGF-β stimulation were quantified (normalized to the corresponding input lysate) and statistical significance assessed (normality was confirmed by Shapiro-Wilk test, followed by unpaired Student *t* test). Data were normalized to the maximum abundance of each protein in RNA interactome capture isolates for each replicate. n=3, data shown as average±SEM, significance values of <0.05 are shown to 3 significant figures. Csde1 indicates cold shock domain containing E1; Eif3c, eukaryotic translation initiation factor 3 subunit C; Erk, extracellular-signal regulated kinase; hnRNP H1, heterogeneous nuclear ribonucleoprotein H1; MCEC, mouse cardiac endothelial cell; and Mov10, Helicase Mov10.

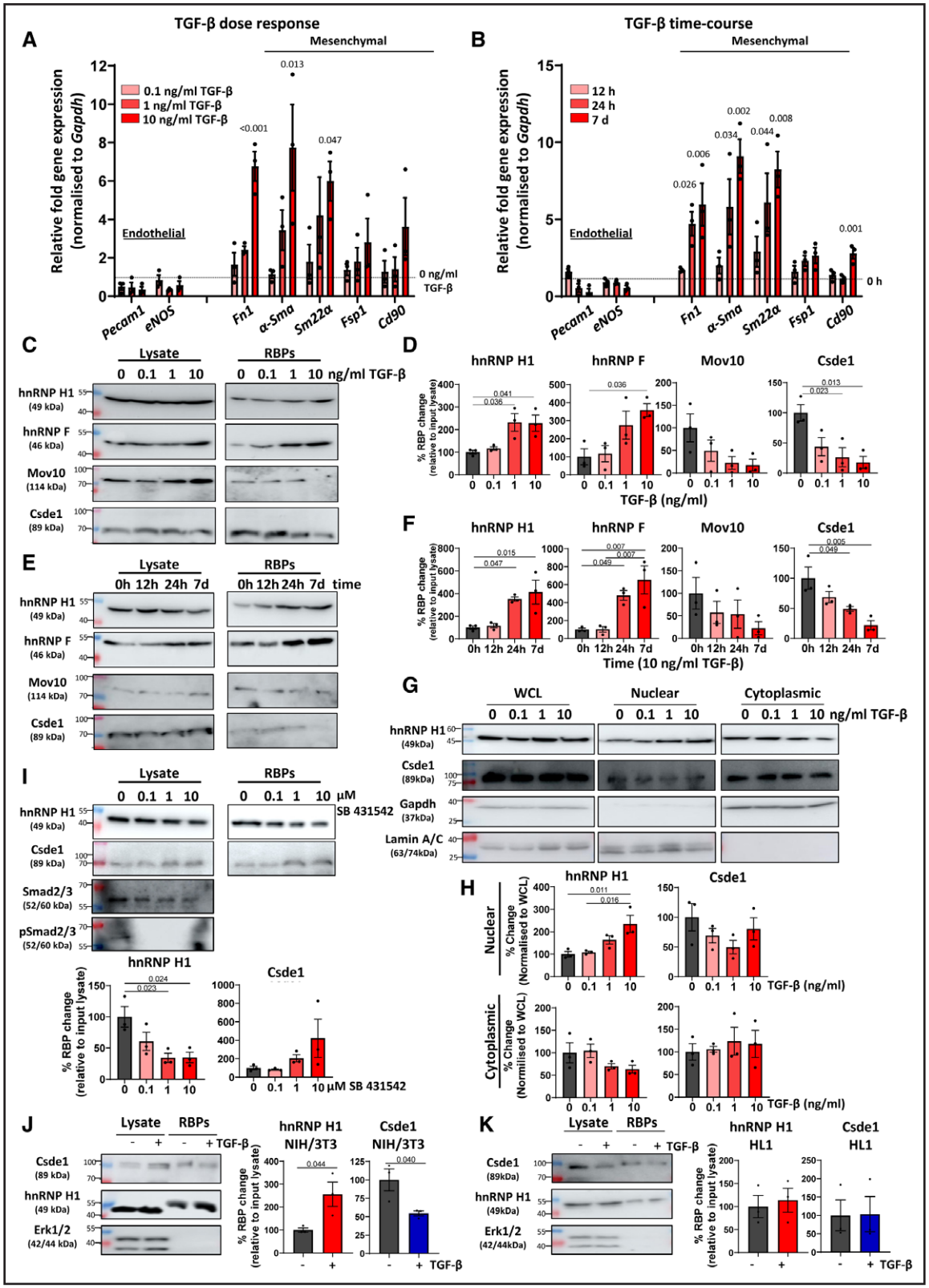

Figure 2. TGF (transforming growth factor)-β dynamically regulates RNA-binding patterns correlating with mesenchymal activation.

A, Effects of TGF-β concentration on endothelial and mesenchymal marker gene expression. Mouse cardiac endothelial cells (MCECs) were incubated in increasing concentrations of TGF-β for 24 hours followed by real-time quantitative polymerase chain reaction (RT-qPCR) assessment of selected endothelial and mesenchymal marker genes. Expression normalized to *Gapdh*, fold change relative to nonstimulated control, n=3, data shown as average±SEM. Data were tested for normality by a Shapiro-Wilk test, and significance was assessed (*Continued*)

50% water) for 30 minutes and washed with water. Gels were treated in 0.02% sodium thiosulphate solution for 10 minutes, washed in water, and then incubated in silver solution (0.1% $AgNO_3$) for 40 minutes. Gels were again washed in water and then incubated in developer solution (1% w/v Na_2CO_3, 0.025% paraformaldehyde) until the desired staining intensity was reached. Stop solution was then added (1% acetic acid) and gels were imaged.

Western Blot

Western blot analysis of proteins was performed according to well-established methodologies. Samples were combined with Laemmli sample buffer, boiled, and separated by SDS-PAGE electrophoresis using 10% polyacrylamide gels along with prestained protein ladder for reference (see Major Resources Table). Following electrophoresis, the proteins were transferred to polyvinylidene fluoride membranes using Biorad Mini Trans-Blot apparatus, blocked for 1 hour in 5% skimmed milk, and incubated with the corresponding primary antibodies (see Major Resources Table) overnight at 4 °C. Blots were subsequently washed in PBS-T, incubated in the corresponding HRP (horse radish peroxidase)-linked secondary antibody (see Major Resources Table) for 1 hour at room temperature before being washed, and visualized by chemiluminescent imaging using an Amersham 680 imager. Western blot images were subsequently uploaded to Licor ImageStudio software (ver 5.2) and quantified using the analysis feature.

Nuclear-Cytoplasmic Fractionation

Nuclear-cytoplasmic fraction was adapted from Suzuki et al,[24] (REAP [Rapid Efficient and Practical]). Briefly, cells (1×10 cm plate per condition) were washed twice in chilled PBS. Cells were then scraped into 1 mL PBS and pelleted by centrifugation. Cells were lysed on 1 mL PBS containing 0.1% IGEPAL CA-630 and input samples were collected. The remaining lysate was briefly centrifuged to pellet nuclear material, and the cytoplasmic fraction was removed to a fresh tube. The nuclear pellet was washed twice in PBS containing 0.1% IGEPAL CA-630 before being suspended in Laemmli sample buffer and homogenized in a Dounce homogenizer.

siRNA Knockdown of hnRNP H1 and Csde1

siRNA (small interfering RNA) knockdowns were performed using ON-TARGETplus (pool of 4) siRNAs (Dharmacon) specific to hnRNP H1 or Csde1 (see oligonucleotides in Major Resources Table). Equivalent concentrations of Silencer Negative Control siRNA (Thermo) were used in control samples. Cells were transfected with 20 nmol/L (MCECs) or 40 nmol/L (HUVECs) siRNA for 48 hours using Lipofectamine RNAiMAX transfection reagent (Thermo Fisher) according to the manufacturer´s instructions unless stated otherwise in the Figure legend. Optimal siRNA conditions were determined by transfection followed by Western blot analyses (Figure S4E).

Figure 2 Continued. by 1-way ANOVA with Dunnett multiple comparison compared with nonstimulated control, significance values of <0.05 are shown to 3 significant figures. **B**, Effects of TGF-β time course on endothelial and mesenchymal marker genes. MCECs were incubated with 10 ng/mL TGF-β for increasing times followed by RT-qPCR assessment of selected endothelial and mesenchymal marker genes. Expression normalized to *Gapdh*, fold change relative to nonstimulated (0 hour) control, n=3, data are shown as average±SEM. Data were tested for normality by a Shapiro-Wilk test, and significance was assessed by 1-way ANOVA with Dunnett multiple comparison compared with nonstimulated control, significance values of <0.05 are shown to 3 significant figures. **C**, Changes in RNA-binding patterns in response to increasing concentrations of TGF-β. MCECs were incubated in increasing concentrations of TGF-β for 24 hours followed by RNA interactome capture (RIC) and Western blot analysis of selected RBPs (RNA-binding proteins). Representative images, n=3. **D**, Quantification of changes in RNA-binding patterns in response to increasing concentrations of TGF-β. Western blots (as shown in **C**) were quantified, RBP abundance was normalized to input lysate for each replicate. Data were tested for normality by a Shapiro-Wilk test, and significance was assessed by 1-way ANOVA with Tukey multiple comparison test, n=3, data shown as average±SEM, significance values of <0.05 are indicated to 3 significant figures. **E**, Changes in RNA-binding patterns in response to TGF-β time course. MCECs were incubated in TGF-β (10 ng/mL) for increasing times followed by RIC and Western blot analysis of selected RBPs. Representative images, n=3. **F**, Quantification of changes in RNA-binding patterns in response to TGF-β time course. Western blots (as shown in **E**) were quantified, RBP abundance was normalized to input lysate for each replicate. Data were tested for normality by a Shapiro-Wilk test, and significance was assessed by 1-way ANOVA with Tukey multiple comparison test, n=3, data shown as average±SEM, significance values of <0.05 are indicated to 3 significant figures. **G**, Changes in nuclear/cytoplasmic location in response to increasing TGF-β. MCECs were incubated in increasing TGF-β (24 hours) followed by nuclear-cytoplasmic fractionation and Western blot analysis. GAPDH was used as a cytoplasmic fraction marker and Lamin A/C as a nuclear fraction marker. Representative blots, n=3. **H**, Quantification of changes in nuclear/cytoplasmic location in response to increasing TGF-β concentrations. Relative changes in the nuclear and cytoplasmic distribution of hnRNP H1 (heterogeneous nuclear ribonucleoprotein H1) and Csde1 (cold shock domain containing E1) were quantified from Western blot analysis (as in **G**). Quantified signal was normalized to the expression in corresponding whole cell lysate (WCL), data were tested for normality by a Shapiro-Wilk test, and significance was assessed by 1-way ANOVA with Tukey multiple comparison test, n=3, data shown as average±SEM, significance values of <0.05 are indicated to 3 significant figures. **I**, Effects of TGF-β receptor inhibition on RNA-binding patterns. MCECs were incubated in TGF-β (10 ng/mL) in the presence of increasing concentrations of the ALK inhibitor SB 431542 (selective ALK4/5/7 inhibitor) for 24 hours followed by RIC and Western blot. RNA-binding (relative to input lysate) was quantified, and significance was assessed by 1-way ANOVA, n=3, data shown as average±SEM. *P<0.05, **P<0.01, ***P<0.001. **J**, Effects of TGF-β on RNA-binding in fibroblasts. NIH/3T3 fibroblast cells were incubated with TGF-β (10 ng/mL) for 24 hours followed by RIC and Western blot analysis. Data were normalized to the maximum abundance of each protein in RNA interactome capture isolates for each replicate, n=3, data shown as average±SEM, normality was confirmed by Shapiro-Wilk test and significance assessed by unpaired Student *t* test, significance values indicated to 3 significant figures. **K**, Effects of TGF-β on RNA-binding in cardiomyocytes. HL1 cardiomyocyte cells were incubated with TGF-β (10 ng/mL) for 24 hours followed by RIC and Western blot analysis. RBP abundance was normalized to input lysate for each replicate. n=3, data shown as average±SEM, normality was confirmed by Shapiro-Wilk test, and significance was assessed by unpaired Student *t* test. ALK indicates anaplastic lymphoma kinase; Mov10, Helicase Mov10; pSmad, phosphorylated-Smad; and Smad, suppressor of mothers against decapentaplegic.

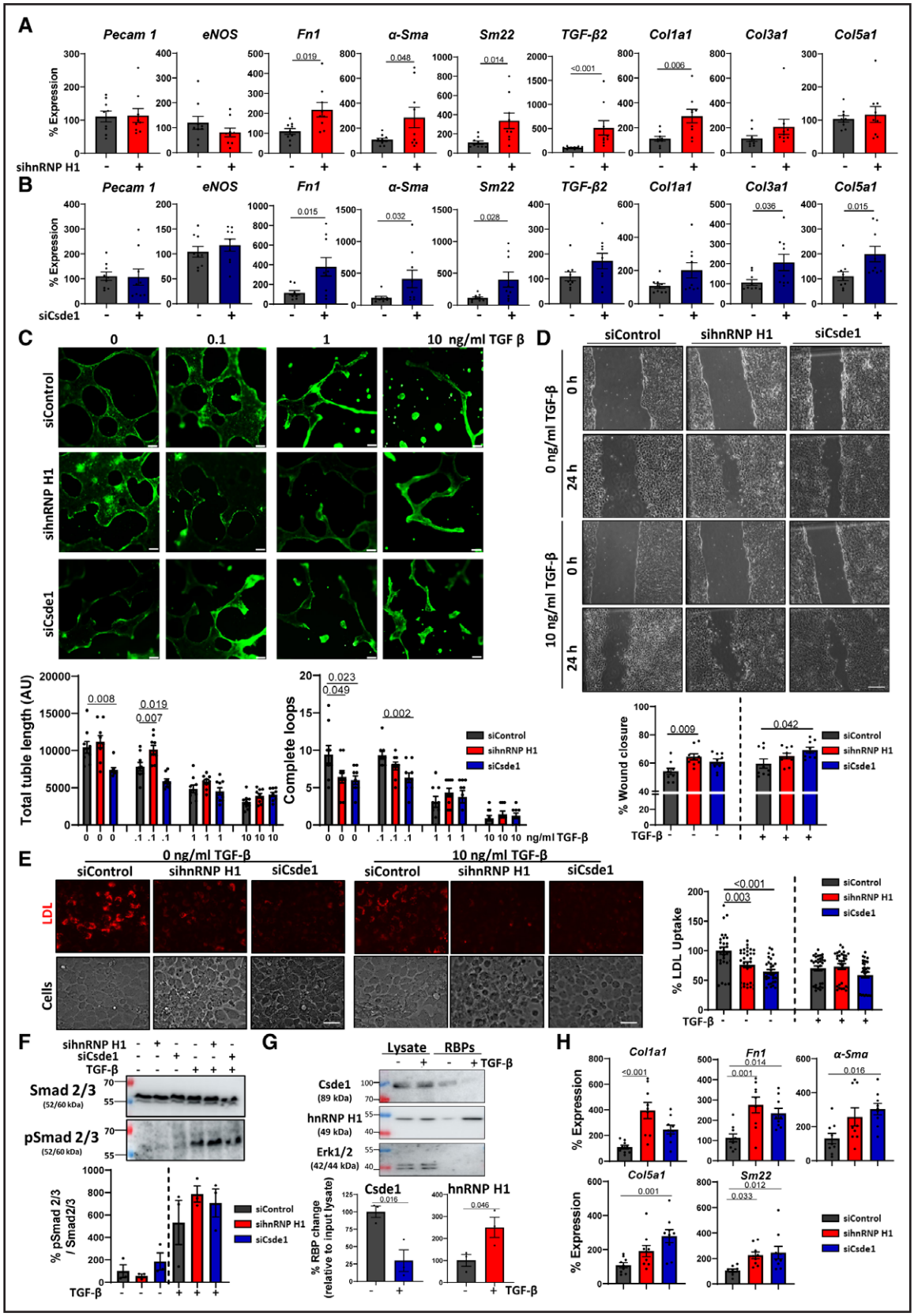

Figure 3. The impact of hnRNP H1 (heterogeneous nuclear ribonucleoprotein H1) and Csde1 (cold shock domain containing E1) on endothelial function and mesenchymal activation.

A, Effects of hnRNP H1 knockdown on endothelial and mesenchymal marker expression. hnRNP H1 was knocked down by siRNA transfection (48 hours) followed by RNA isolation and real-time quantitative polymerase chain reaction (RT-qPCR) analysis of selected marker (*Continued*)

hnRNP H1 and Csde1 Overexpression

hnRNP H1 and Csde1 overexpression experiments were performed using either hnRNP H1 or Csde1 mouse open reading frame constructs expressing the proteins downstream of a CMV promoter, which were purchased from Origene (see Major Resources Table). Equivalent concentrations of an empty vector control were transfected in control samples. Plasmids were transfected for 48 hours using a Lipofectamine 3000 transfection reagent kit (Thermo Fisher) according to manufacturer´s instructions. Overexpression was validated by transfection followed by real-time quantitative polymerase chain reaction (qPCR; Figure S4G).

RNA Isolation and Real-Time qPCR

RNA was isolated from cells using the NucleoSpin RNA extraction kit (Macherey-Nagel) according to the manufacturer´s instructions. RNA was reverse transcribed using the Maxima H Minus First Strand cDNA Synthesis Kit (Thermo Fisher Scientific) with oligo d(T) and random hexamer primers according to the manufacturer´s instructions. qPCR was performed according to well-established methodologies using the Maxima Sybr qPCR kit (Thermo Fisher Scientific). The relative amount of target gene expression was normalized to *Gapdh* levels unless otherwise stated in the Figure legend (Figures 5 and 7). Relative changes in RNA abundance between experimental conditions were compared using the $2^{-\Delta\Delta Ct}$ method and expressed as a percentage of control expression unless stated otherwise in the Figure legend (Figures 5 and 7).

EC Isolation From Adult Mouse Heart

Hearts after TAC were washed in PBS, minced, and digested in collagenase I (500 U/mL) and DNase I (150 U/mL) in RPMI (Roswell Park Memorial Institute) 1640 media for 1 hour at 37 °C. Digested samples were filtered through a 0.7 µm cell strainer and washed 4× in FCS followed by 4 washes in MACS (magnetic-activated cell sorting) buffer with BSA (bovine serum albumin). Samples were resuspended in MACS buffer and then incubated with CD146 beads for 30 minutes at 4 °C. Bound cells were collected on magnetic columns. Columns were washed in MACS buffer (3×). Beads were flushed into a fresh column and washes were repeated. Following this, beads were flushed into a fresh tube and pelleted by centrifugation.

RNA Stability Assay

MCECs were cultured in 12 well plates under the experimental conditions as described in the respective Figure legends. Actinomycin D was added directly to the culture medium at a final concentration of 10 µg/mL for the time periods indicated, followed by RNA isolation and qPCR as described.

Figure 3 Continued. gene expression. Expression normalized to *Gapdh,* n=3, each in triplicate, data shown as average±SEM. Normality was tested by a Shapiro-Wilk test, significance of normally distributed data was assessed by unpaired Student *t* test (transforming growth factor [*TGF*]-*β2* expression was tested by Mann-Whitney *U* test). Significance values of <0.05 are shown as 3 significant figures. **B**, Effects of Csde1 knockdown on endothelial and mesenchymal marker expression. Csde1 was knocked down by siRNA transfection (48 hours) followed by RNA isolation and RT-qPCR analysis of selected marker gene expression. Expression normalized to *Gapdh,* n=3, each in triplicate, data shown as average±SEM. Normality was tested by a Shapiro-Wilk test, significance of normally distributed data were assessed by unpaired Student *t* test *(Sma* and *Col5a1* expression was tested by Mann-Whitney *U* test). Significance values of <0.05 are shown to 3 significant figures. **C**, Effects of hnRNP H1 and Csde1 knockdown on tubule formation. hnRNP H1 and Csde1 were knocked down (siRNA, 48 hours) in increasing concentrations of TGF-β (24 hours). Cells were plated onto Matrigel matrix for 24 hours; BCECF was added and tubule formation was assessed by fluorescent microscopy. Quantifications represent average total tubule length and number of complete loops per visible field. Representative images (n=3 triplicates/condition, scale bar 100 µm). Data shown as average±SEM, normality was assessed by Shapiro-Wilk test, and significance was assessed by 1-way ANOVA with Dunnett test for multiple comparisons. Significance values shown to 3 significant figures. **D**, Effects of hnRNP H1 and Csde1 on endothelial cell migration. Mouse cardiac endothelial cells (MCECs) were incubated with si-hnRNP H1 or siCsde1 for 48 hours in the presence and absence of TGF-β stimulation (10 ng/mL, 24 hours). Migration was assessed 24 hours after scratching. Representative images, n=3 triplicates/condition, data shown as average±SEM, normality was assessed by Shapiro-Wilk test, and significance assessed by 1-way ANOVA with Dunnett test for multiple comparisons. Significance values shown to 3 significant figures. **E**, Effects of hnRNP H1 and Csde1 knockdown on LDL (low-density lipoprotein) uptake. hnRNP H1 and Csde1 were knocked down (siRNA, 48 hours)±TGF-β stimulation (10 ng/mL, 24 hours). Cells were incubated in fluorescently labeled LDL and uptake was assessed by fluorescence microscopy. Representative images (n=3, scale bar 50 µm). Data shown as average±SEM. n=3 (10 quantifications per replicate), normality was assessed by Shapiro-Wilk test, and significance was assessed by 1-way ANOVA with Dunnett test for multiple comparisons. Significance values are shown to 3 significant figures. **F**, Effects of hnRNP H1 and Csde1 knockdown on Smad2/3 phosphorylation. MCECs were incubated with si-hnRNP H1 or siCsde1 for 48 hours in the presence and absence of TGF-β stimulation (10 ng/mL, 24 hours). Smad 2/3 phosphorylation was assessed by Western blot (relative to total Smad 2/3 expression). Representative blot. n=3, data shown as average±SEM. Normality was assessed by Shapiro-Wilk test, and significance was assessed by 1-way ANOVA with Dunnett test for multiple comparisons (no significance). **G**, Validation of TGF-β driven changes in RNA-binding in primary human cardiac microvascular endothelial cells (HCMECs). HCMECs were incubated with TGF-β (10 ng/mL) for 24 hours followed by RNA interactome capture (RIC) and Western blot analysis. RBPs (RNA-binding proteins) abundance was normalized to input lysate for each replicate. n=3, data shown as average±SEM, normality was confirmed by Shapiro-Wilk test and significance assessed by unpaired Student *t* test, significance values are shown to 3 significant figures. **H**, Validation of changes in mesenchymal maker gene expression after hnRNP H1 and Csde1 knockdown in HCMECs. hnRNP H1 and Csde1 were knocked down in HCMECs by siRNA transfection (48 hours) followed by RNA isolation and RT-qPCR analysis of selected marker gene expression. n=3, each in triplicate, data were tested for normality by a Shapiro-Wilk test and significance assessed by 1-way ANOVA with Dunnett multiple comparison test, data shown as average±SEM, significance values of <0.05 are indicated to 3 significant figures. BCECF indicates 2',7'-bis-(2-carboxyethyl)-5-(and-6)-carboxyfluorescein, acetoxymethyl ester; siControl, control siRNA; siCsde1, siRNA targeting Csde1; sihnRNP H1, siRNA targeting hnRNP H1; siRNA, small interfering RNA; Smad, suppressor of mothers against decapentaplegic; and pSmad, phosphorylated-Smad.

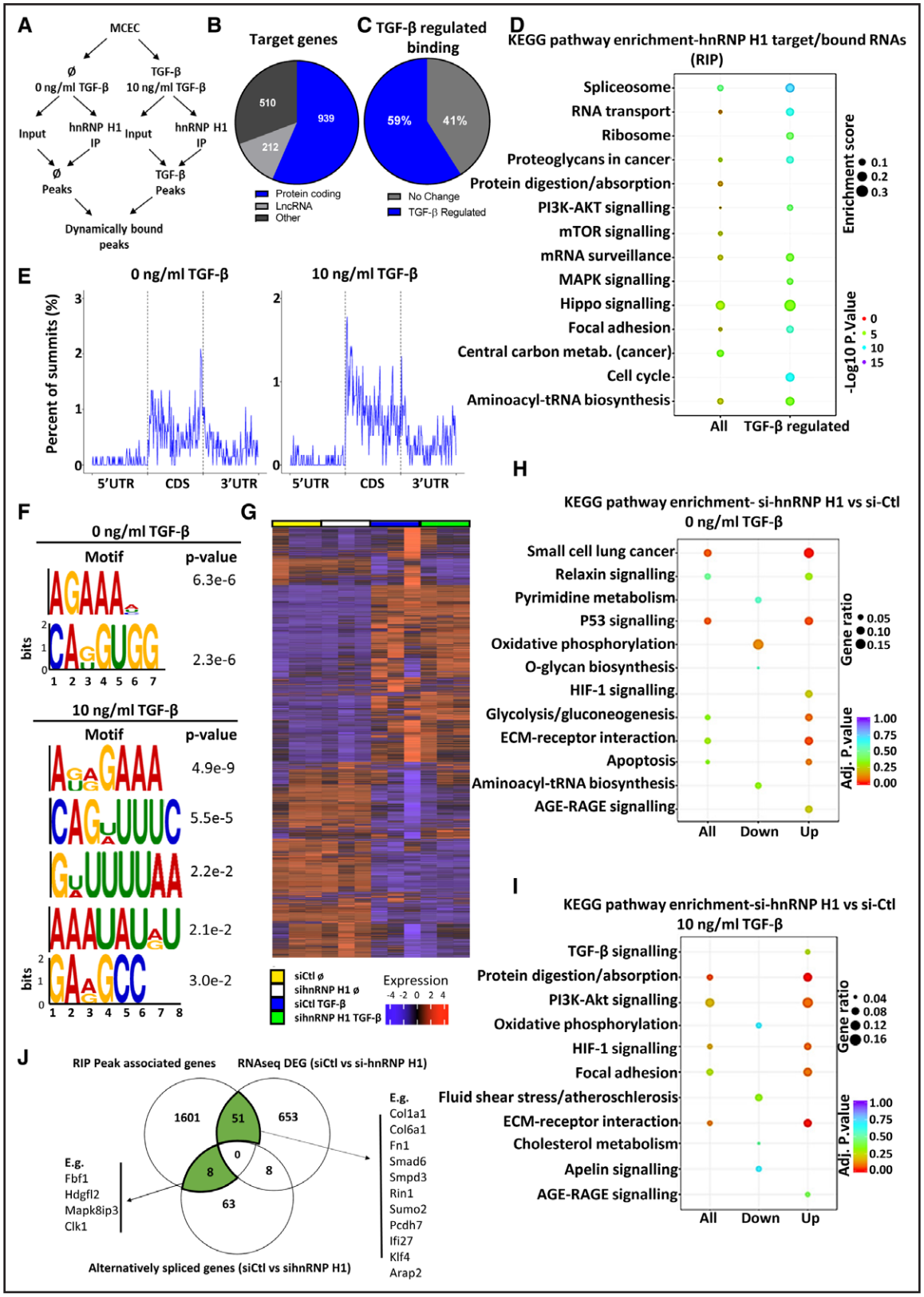

Figure 4. Identification of the dynamically bound target RNAs of hnRNP H1 (heterogeneous nuclear ribonucleoprotein H1) using RNA immunoprecipitation sequencing (RIP-seq) and RNA-sequencing (RNA-seq).

A, Schematic overview of RIP-seq design. Libraries were generated from input and hnRNP H1 immunoprecipitation (IP) samples±TGF (transforming growth factor)-β stimulation to identify global and TGF-β–regulated binding patterns of hnRNP H1. **B**, Target RNAs of hnRNP H1. Proportion peak-associated genes identified as targets of hnRNP H1, sorted by gene type. **C**, Proportion of TGF-β–regulated binding. Proportion of hnRNP H1 target genes differentially bound after TGF-β stimulation ($P<0.05$). **D**, Pathway enrichment of hnRNP H1 (*Continued*)

Tubule Formation

MCECs or HUVECs were treated under the respective conditions and plated (25 000 cells per well) onto a 96-well plate which had been precoated in Corning Matrigel basement membrane. Cells were incubated for 24 hours under standard culture conditions. Thirty minutes before imaging, tubules were fluorescently labeled by the addition of 1:5000 0.1% BCECF AM Ester (2',7'-bis-(2-carboxyethyl)-5-(and-6)-carboxyfluorescein, acetoxymethyl ester), and tubule formation was imaged using fluorescent microscopy. Tubule formation was quantified by measuring the total tubule length and number of complete loops in the visible field using Image J software.

Migration Assay

MCECs were plated onto 6 well plates, marked with a grid on the underside, and incubated under the respective experimental conditions. Following this, Mitomycin C was added to media to a final concentration of 10 µg/mL for 2 hours. Cells were then scratched with a sterile tip along the grid, washed twice in PBS, and media was replaced. Migration was assessed by analyzing scratch closure after 24 hours using Image J software.

Low-Density Lipoprotein Uptake

LDL (low-density lipoprotein) uptake in MCECs was assessed using an Abcam cell-based LDL-uptake assay kit according to the manufacturer's instructions. Relative LDL uptake was quantified by measuring changes in the relative fluorescence intensity, following microscopy, using ImageJ software.

RNA Immunoprecipitation

RIP was adapted from Gagliardi and Matarazzo.[25] Cells (4×10 cm plates) were washed in chilled PBS and scraped into 400 µL RIP lysis buffer (100 mmol/L KCl, 5 mmol/L MgCl2, 10 mmol/L HEPES pH 7, 0.5% IGEPAL CA-630, 0.1 mmol/L DTT, 1×protease inhibitor cocktail, 1×RNasIN). Lysates were vortexed and homogenized by passing through a 21 gauge needle. Fifty microliters of Biorad Protein A magnetic Surebeads were coupled to 5 µg anti–hnRNP H1 or anti-Csde1 antibody overnight at 4 °C. Ten percent of lysate samples were removed as input and placed on ice. Antibody coupled beads were washed twice in NT2 buffer (50 mmol/L Tris-HCl pH 7.4, 150 mmol/L NaCl, 5 mmol/L MgCl2, 0.05% IGEPAL CA-630) and resuspended in 660 µL NET-2 buffer (50 mmol/L Tris-HCl pH 7.4, 150 mmol/L NaCl, 5 mmol/L MgCl2, 0.05% IGEPAL CA-630, 20 mmol/L EDTA pH 8, 1 mmol/L DTT, 1×RNaseIN). Lysate was added to beads and incubated for 2 hours at 4 °C.

Supernatant was removed from beads, which were then washed 5× in ice-cold NT2 buffer. Beads were resuspended in 150 µL Proteinase K buffer (50 mmol/L Tris-HCl pH 7.4, 150 mmol/L NaCl, 5 mmol/L MgCl2, 0.05% IGEPAL CA-630, 1% SDS; at this stage, conditions of input samples were adjusted and processed in parallel to immunoprecipitation samples). Twenty microliters of proteinase K was added and samples were incubated at 55 °C for 30 minutes. Supernatants were transferred to a fresh tube and combined with 230 µL NT2 buffer. Four hundred microliters of phenol chloroform was added and samples were centrifuged through a heavy-lock tube. The aqueous phase was removed and the RNA was purified using a Zymo RNA clean and concentrator kit according to the manufacturer's instructions. Following this, purified RNA was DNase digested using TurboDNase (Thermo) according to manufacturer's instructions and repurified with a Zymo RNA clean and concentrator kit.

RIP-Sequencing Analysis

RNA quality was assessed using an Agilent 2100 bioanalyser to determine RNA concentration and fragment size distribution, followed by agarose gel electrophoresis to determine sample purity. Following successful quality control, RNA was fragmented into fragments of ≈250 bases. Fragments were reverse transcribed using random primers and cDNAs were dA-tailed. Tailed DNA fragments were ligated to sequencing adaptors and the final DNA library was obtained by PCR amplification. Following library construction, initial quantification was performed with Qubit 2.0, and the library was diluted to 1 ng/L. Sequencing was performed using the Illumina NovaSeq platform. The raw data from the Illumina platform was transformed into Sequenced Reads with the Illumina CASAVA [Consensus Assessment of Sequence and Variation] v1.8 software. Resulting FASTQ files were quality-controlled using FASTQC.

Following quality control, raw data were trimmed to remove adaptor sequences and low-quality bases using the skewer platform. Trimmed fragments were mapped to the reference genome using the BWA (Burrow-Wheeler Aligner) platform.

Figure 4 Continued. targets. Enriched terms (KEGG pathway) among all peak-related genes (all targets) and differentially bound peak-related genes (TGF-β–regulated binding). **E**, mRNA summit location. The proportion of summit locations identified within mRNA targets±TGF-β stimulation (from averaged replicates). **F**, Predicted binding motifs of hnRNP H1. Significantly enriched motifs were identified in peaks in the presence or absence of TGF-β stimulation. **G**, Heatmap of effects of hnRNP H1 knockdown on RNA expression. RNA-seq after siRNA knockdown (48 hours) of hnRNP H1 in the absence (0 ng/mL TGF-β, siCtl_NS vs sihnRNP_NS) or presence (10 ng/mL TGF-β, siCtl_TGF vs sihnRNP_TGF) of TGF-β stimulation. **H**, Pathway enrichment of differentially expressed genes si-Ctl vs si-hnRNP H1 in nonstimulated cells. Pathway enrichment among all differentially expressed genes, upregulated and downregulated genes in si-hnRNP H1 samples compared with si-Ctl samples in the absence of TGF-β stimulation. **I**, Pathway enrichment of differentially expressed genes si-Ctl vs si-hnRNP H1 in TGF-β stimulated cells. Pathway enrichment among all differentially expressed genes, upregulated and downregulated genes in si-hnRNP H1 samples compared with si-Ctl samples in the presence of TGF-β stimulation. **K**, Overlap between RIP-seq and RNA-seq. The overlap between peak-associated genes identified as targets of hnRNP H1 (RIP-seq) compared with differentially expressed genes (si-Ctl- vs si-hnRNP H1, $P<0.05$ RNA-seq) and genes with significant alternative splicing (si-Ctl- vs si-hnRNP H1, $P<0.05$ RNA-seq). AGE-RAGE indicates advanced glycation end-products-receptor for AGE; CDS, coding sequence; DEG, differentially expressed gene; ECM, extracellular matrix; HIF, hypoxia inducible factor; KEGG, Kyoto Encyclopedia of Genes and Genomes; lncRNA, long noncoding RNA; MAPK, mitogen-activated protein kinase; MCEC, mouse cardiac endothelial cell; metab., metabolism; mTOR, mammalian target of rapamycin; siCtl_NS and siCtl_TGF, control siRNA nonstimuated and control siRNA TGF-β stimulated; sihnRNP_NS and sihnRNP_TGF, hnRNP H1 siRNA nonstimulated and hnRNP H1 siRNA TGF-β stimulated; siRNA, small interfering RNA; tRNA, transfer RNA; and UTR, untranslated region.

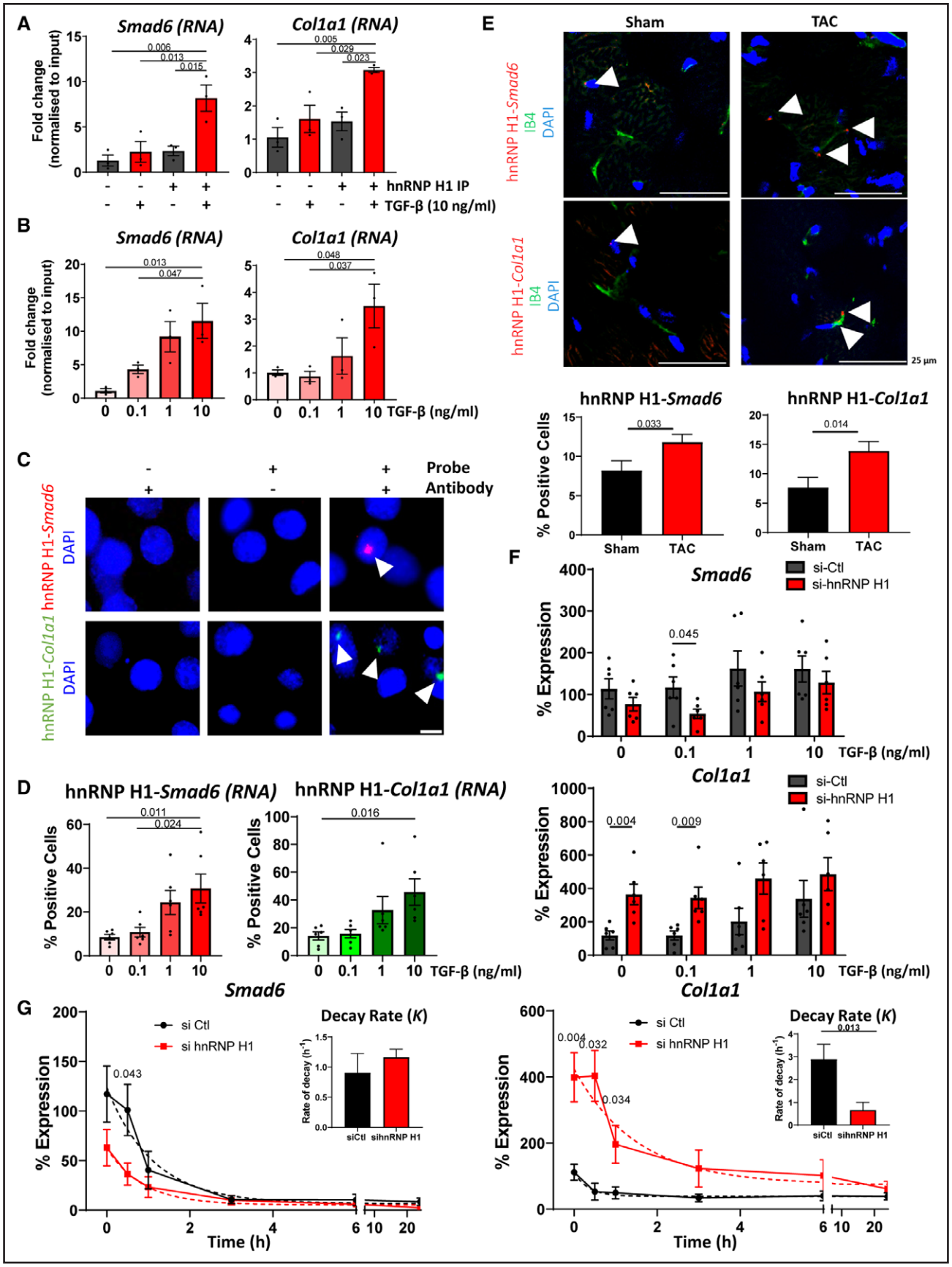

Figure 5. Characterization of the interactions between RNA and hnRNP H1 (heterogeneous nuclear ribonucleoprotein H1).
A, RNA immunoprecipitation (RIP) validation of binding to target RNAs. Quantitative polymerase chain reaction (qPCR) analysis (*Continued*)

Duplicate reads were labeled using SAMBLAST, and mapping quality was calculated using MAPQC ($P<0.05$ mapping threshold). rRNA (ribosomal RNA; common contaminants of RIP sequencing) were removed using bowtie.

For specific binding sites, their enrichment in immunoprecipitation samples compared with input was used to predict the site of RNA-protein interaction. MACS2 (Model-Based Analysis of ChIP-seq) software was used to calculate the enrichment level of reads per window and predict the length of fragment sizes for mapping results and peak calling to map enriched peaks to the reference sequence. Peaks were identified that were significantly enriched in immunoprecipitation samples compared with matched inputs using MACS2 and diffbind ($P<0.05$, FC [fold change] >2). Analysis of differential abundance of peak-associated genes between conditions was performed using diffbind. As peak distribution can predict binding sites, MEME software was used to identify and map significantly enriched binding motifs. Peak-related genes were analyzed for KEGG (Kyoto Encyclopedia of Genes and Genomes) pathway enrichment using KOBAS (KEGG Orthology Based Annotation System) software, and GO (gene ontology) enrichment was calculated using GOSeq/TopGO software packages.

RNA Sequencing

Following RNA isolation, mRNA was purified using poly T magnetic beads. RNA was fragmented and cDNA synthesized using random primers, followed by second-strand cDNA synthesis, end repair, A-tailing, adaptor ligation, size selection, amplification, and purification. The library was checked with Qubit and real-time PCR for quantification and Bioanalyser for size distribution detection. Quantified libraries were pooled and sequenced on the Illumina NovaSeq platform. Raw data were processed to remove low-quality reads and adaptor sequences.

High-quality data were aligned to the reference genome using Hisat2 software. The number of reads mapped to each gene was calculated using featureCounts. Differential expression analysis was performed using DESeq2 software; genes with an adjusted $P<0.05$ were assigned as differentially expressed. KEGG and GO enrichment were performed for RIP sequencing. Alternative splicing analysis was performed using rMATS software.

Proximity Ligation Assay

Specific single-stranded DNA probes were designed complementary to specific targets of hnRNP H1 and Csde1 using Stellaris Probe Designer. Probes were designed as 20 to 24 mers and incorporated a 3' biotin tag. Four specific probes for each target were pooled, which were selected based on their proximity to RIP-related peaks identified for the target, proximity to predicted binding motifs, and region within the target RNA.

Cells or tissue samples were fixed in 4% paraformaldehyde, washed in PBS, and permeabilized in PBS containing 1% BSA and 0.1% TritonX100. Cells were washed in 0.1M triethanolamine, and acetic anhydride was gradually added to a final concentration of 0.5%. Cells were washed in PBS-Tween20 (0.02%) followed by washing in hybridization buffer (5×SSC [saline-sodium citrate], 1×Denhardts reagent, 0.1% Tween20, 0.1% CHAPS [3-[(3-cholamidopropyl)dimethylammonio]-1-propanesulfonate], 5 mM EDTA, 1 mg/mL RNase free tRNA [transfer RNA], 100 µg/mL heparin). Probes (200 nmol/L final concentration) were boiled at 95 °C and incubated with cells in hybridization buffer overnight at 37 °C in a humidity chamber. Next, slides were washed sequentially in buffers in the following order; 50% deionized formamide/5×SSC, 25% deionized formamide/1×SSC, 12.5% deionized formamide/2×SSC, 2×SSC/0.1% Tween20 and 0.2×SSC/0.1% Tween20. Slides were washed in PBS-Tween20 (0.02%) and blocked in Duolink

Figure 5 Continued. of the enrichment of *Smad6* and *Col1a1* RNA in hnRNP H1 immunoprecipitation (IP) samples ± TGF (transforming growth factor)-β stimulation (10 ng/mL, 24 hours) compared with IgG controls (IP–). Normalized to input expression. n=3, data shown as average±SEM, normality tested by Shapiro-Wilk test, significance assessed by 1-way ANOVA with Tukey multiple comparison test, significance shown to 3 significant figures. **B**, Effects of TGF-β on target binding. qPCR analysis of *Smad6* and *Col1a1* abundance in hnRNP H1 IPs in the presence of increasing concentrations of TGF-β stimulation (24 hours). Abundance relative to input, n=3, data shown as average±SEM, normality tested by Shapiro-Wilk test, significance assessed by 1-way ANOVA with Tukey multiple comparison test, significance shown to 3 significant figures. **C**, Validation of interactions in situ by proximity ligation assay (PLA) assay. PLA assay in mouse cardiac endothelial cells (MCECs) showing the interaction between hnRNP H1 and *Smad6* (red) or *Col1a1* (green) RNA. Representative image, scale bar 10 µm **D**, Effects of TGF-β stimulation on hnRNP H1 interactions. Quantifications of hnRNP H1 interaction with *Smad6* or *Col1a1* RNA after stimulation with increasing concentrations of TGF-β (24 hours). Normality assessed by Shapiro-Wilk test, significance assessed by 1-way ANOVA with Tukey multiple comparison, significance shown to 3 significant figures, data shown as average±SEM. **E**, Validation of interactions in vivo. PLA assay of the interaction of hnRNP H1 with *Smad6* (**top**) or *Col1a1* (**bottom**; interactions red) in mouse heart sections 2 weeks following sham or transverse aortic constriction (TAC) surgery. IB4 (green) shows endothelial cells, nuclei are stained with DAPI (blue). Representative images, scale bar 25 µm. Arrowheads point to positive interactions. Graphs show number of interactions normalized to the number of cells per visible field. Error data shown as average±SEM. Normality was assessed by Shapiro-Wilk test, significance was assessed by unpaired Student *t* test, and significance was shown to 3 significant figures. **F**, Effects of hnRNP H1 on *Smad6* and *Col1a1* expression. qPCR analysis of changes in *Smad6* and *Col1a1* abundance following TGF-β stimulation and si-hnRNP H1 knockdown. Normalized to *Gapdh* expression, n=6, data shown as average±SEM, normality assessed by Shapiro-Wilk test, and significance was assessed by unpaired Student *t* test between si-hnRNP H1 and si-control conditions significance shown to 3 significant figures. **G**, Effects of hnRNP H1 on RNA stability. hnRNP H1 was knocked down with siRNA for 48 hours before addition of Actinomycin D 10 µg/mL to inhibit transcription. RNA abundance was measured by real-time quantitative polymerase chain reaction (normalized to *Gapdh)* and a nonlinear regression curve was calculated to assess effects on RNA stability. n=6, data shown as average±SEM, normality assessed by Shapiro-Wilk, and significance was assessed by unpaired Student *t* test between corresponding conditions, significance shown to 3 significant figures. Bar charts show the averaged decay constant, **K**, ±SEM, of each nonlinear regression curve with significance assessed by unpaired Student *t* test, significance shown to 3 significant figures. DAPI indicates 4′,6-diamidino-2-phenylindole; IB4, isolectin B4; si-Ctl, control siRNA; si-hnRNP H1, hnRNP H1 siRNA; and siRNA, small interfering RNA.

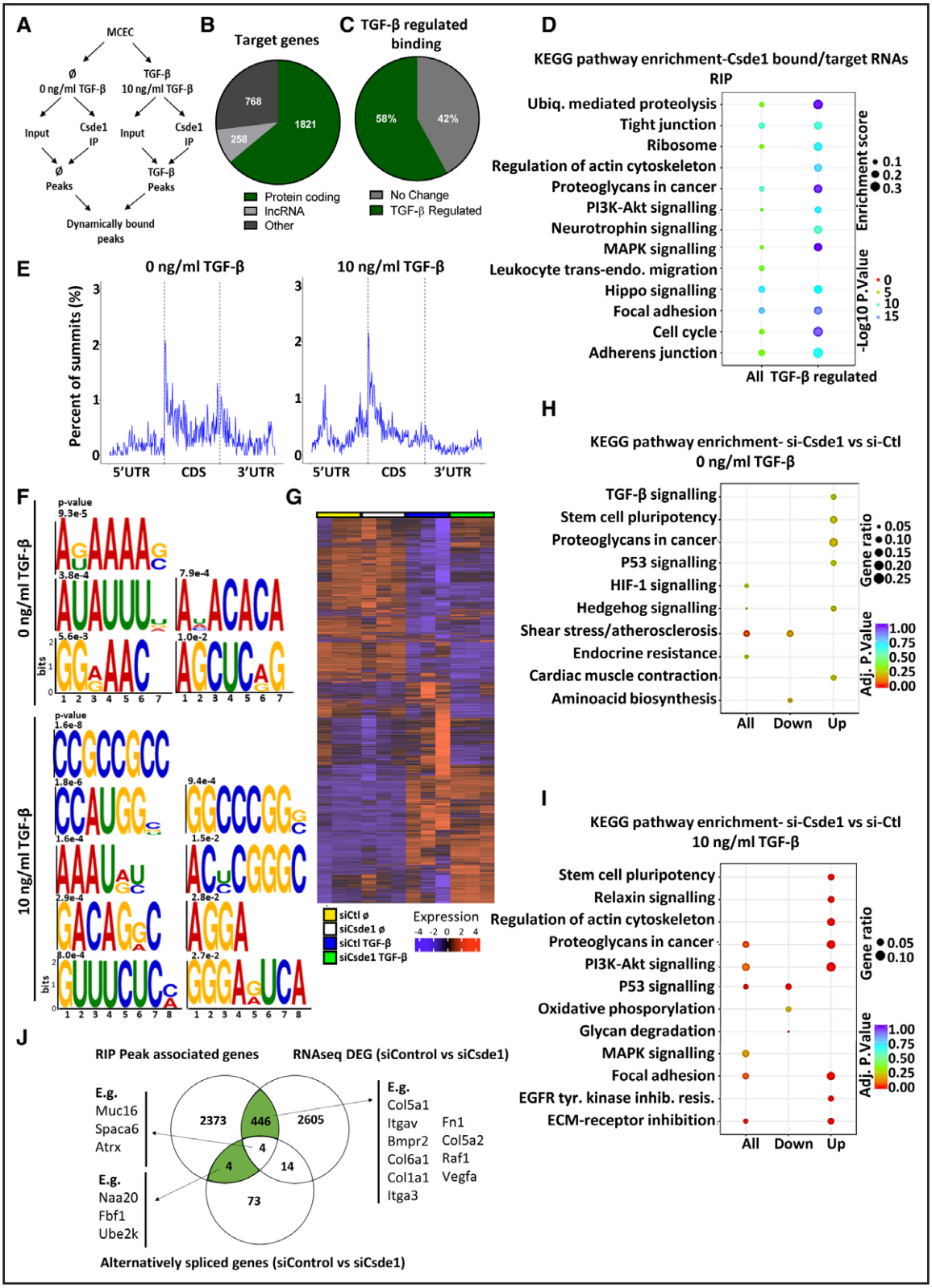

Figure 6. Identification of the functional TGF (transforming growth factor)-β–regulated targets of Csde1 (cold shock domain containing E1) using RNA immunoprecipitation sequencing (RIP-seq) and RNA-sequencing (RNA-seq).

A, Schematic overview of RIP-seq design. Libraries were generated from input and Csde1 immunoprecipitation (IP) samples in the presence and absence of TGF-β stimulation to identify global and TGF-β–regulated binding patterns of Csde1. **B**, Target transcripts of Csde1. The number peak associated genes identified as targets of Csde1, sorted by gene type. **C**, Proportion of TGF-β–regulated binding. Proportion of the target genes of Csde1, which were differentially bound after TGF-β stimulation ($P<0.05$). **D**, Pathway enrichment of Csde1 targets. Enriched terms (KEGG pathway) among all peak-related genes (all targets) and all differentially bound peak-related genes (TGF-β–(*Continued*)

blocking buffer. Primary antibodies (Rabbit-anti hnRNP H1 or Csde1 and Mouse-anti biotin) were diluted in Duolink antibody dilutent and incubated overnight at 4 °C.

Slides were washed in Duolink buffer A, and Duolink probes (Rabbit MINUS and Mouse PLUS) were incubated with slides for 1 hour at 37 °C. Slides were washed in buffer A and incubated in Duolink ligase mix for 30 minutes at 37 °C then polymerase/amplification mix for 100 minutes at 37 °C. Slides were washed in buffer B followed by 0.01% buffer B and mounted in Vectashield Mounting Medium with DAPI (for tissue samples an additional incubation in fluorescein-labeled isolectin B4 antibody was performed before mounting). Proximity ligation assay (PLA) specificity was validated by performing the PLA in the absence of PLA probe with normal primary antibody, and with the PLA probe in the absence of primary antibody. The staining specificity of hnRNP H1 and Csde1 was validated alongside the corresponding IgG control before PLA.

Immunofluorescence and PLA Imaging

All immunofluorescence images were examined and captured with a DMi8 Leica microscope in High-Power field. In addition, PLA images for in vivo samples were imaged on confocal TCS SP8 Leica microscope with a ×40/1.25 oil objective.

Quantification and Statistical Analysis

All data are shown as mean±SEM. Before statistical testing, normality (Gaussian distribution) was tested by a Shapiro-Wilk test. Data were assumed as normality distributed with a $P>0.05$. When data were normally distributed, statistical significance was assessed using an unpaired Students *t* test (when comparison was made between 2 experimental groups) or a 1-way ANOVA with multiple comparisons and a post hoc test to compare significance between groups (either a Dunnett multiple group test was used to compare significance with the control group, or Tukey multiple comparison test was used to assess significance between all groups; when comparison was made between 3 or more experimental groups) as indicated in the Figure legend. $P<0.05$ were considered statistically significant throughout and are shown in Figure to 3 significant figures. Data that were not normally distributed (Shapiro-Wilk $P<0.05$) was analyzed for significance by a Mann-Whitney *U* test or a Kruskal-Wallis test. All significance testing is based on at least 3 independent biological replicates per condition, as stated in the accompanying Figure legends. Significance testing was performed using GraphPad Prism 7 software.

RESULTS

Identification of Endothelial TGF-β–Regulated RBPs

To gain insight into TGF-β stimulated changes in the mRNA-binding patterns of endothelial RBPs, we applied RIC to a mouse cardiac EC line (MCECs). MCECs were incubated in the presence or absence of 10 ng/mL TGF-β stimulation for 24 hours followed by ultraviolet crosslinking, oligo d(T) precipitation, stringent washing, and RBP elution (Figure 1A). We validated the experimental setup after RIC followed by silver staining, showing specific enrichment of RBPs compared with noncrosslinked controls and input lysate (Figure 1B). In the absence of ultraviolet-crosslinking, no covalent link is formed between RNA and bound proteins, and as such proteins are removed during the high-stringency washing steps. Next, RBPs in RIC eluates (n=3) with and without TGF-β stimulation (10 ng/mL, 24 hours), and ultraviolet crosslinking were identified and quantified by tandem mass tag labeling followed by liquid chromatography-mass spectrometry (Table S1). Two hundred sixty-three proteins were identified, of which 247 were significantly enriched in cross-linked versus noncrosslinked controls (false discovery rate, 0.05; fold change ≥2; Figure 1C).

We defined TGF-β–regulated RBPs as those with ≥100% change in RNA binding (relative abundance in RIC isolates) between TGF-β stimulated and unstimulated samples (after excluding proteins without enrichment in cross-linked versus noncrosslinked samples—background), revealing 119 TGF-β–regulated RBPs (Figure 1D). We assessed the proportion of canonical and noncanonical RBPs by comparing our results with the RBPbase data set (https://rbpbase.shiny.embl.de/), annotating RBPs by the presence/absence of a canonical RNA-binding domain or GO RBP annotation (Figure 1E). This showed that the majority of RBPs have GO RBP annotation, although most lack a canonical RNA-binding domain, highlighting RBP diversity. Ontological analysis demonstrated a clear enrichment of RNA-related functions among proteins isolated by RIC under all conditions (Figure S1). To focus on the most significantly TGF-β–regulated RBPs, proteins were sorted by fold change and significance

Figure 6 Continued. regulated binding). **E**, mRNA summit location. The proportion of summit locations identified within mRNA targets in the presence or absence of TGF-β stimulation (from combined replicates). **F**, Binding motifs of Csde1. Significantly enriched binding motifs were identified for Csde1 in the presence or absence of TGF-β stimulation. **G**, Heatmap of effects of Csde1 knockdown on RNA expression. RNA-seq after siRNA knockdown of Csde1 in the absence (0 ng/mL TGF-β, siCtl_NS vs siCsde1_NS) or presence (10 ng/mL TGF-β, siCtl_TGF vs siCsde1_TGF) of TGF-β stimulation. **H**, Pathway enrichment of differentially expressed genes si-Ctl vs si-Csde1 in nonstimulated cells. Pathway enrichment among all differentially expressed genes, upregulated and downregulated genes in si-Csde1 samples compared with si-Ctl samples in the absence of TGF-β stimulation. **I**, Pathway enrichment of differentially expressed genes si-Ctl vs si-Csde1 in TGF-β stimulated cells. Pathway enrichment among all differentially expressed genes, upregulated and downregulated genes in si-Csde1 samples compared with si-Ctl samples in the presence of TGF-β stimulation. **J**, Overlap between RIP-seq and RNA-sequencing (RNA-seq). The overlap between peak-associated genes identified as targets of Csde1 (RIP-seq) compared with differentially expressed genes (si-Ctl- vs si-csde1, $P<0.05$ RNA-seq) and genes with significant alternative splicing (si-Ctl- vs si-Csde1, $P<0.05$ RNA seq). CDS indicates coding sequence; MCEC, mouse cardiac endothelial cell; and UTR, untranslated region.

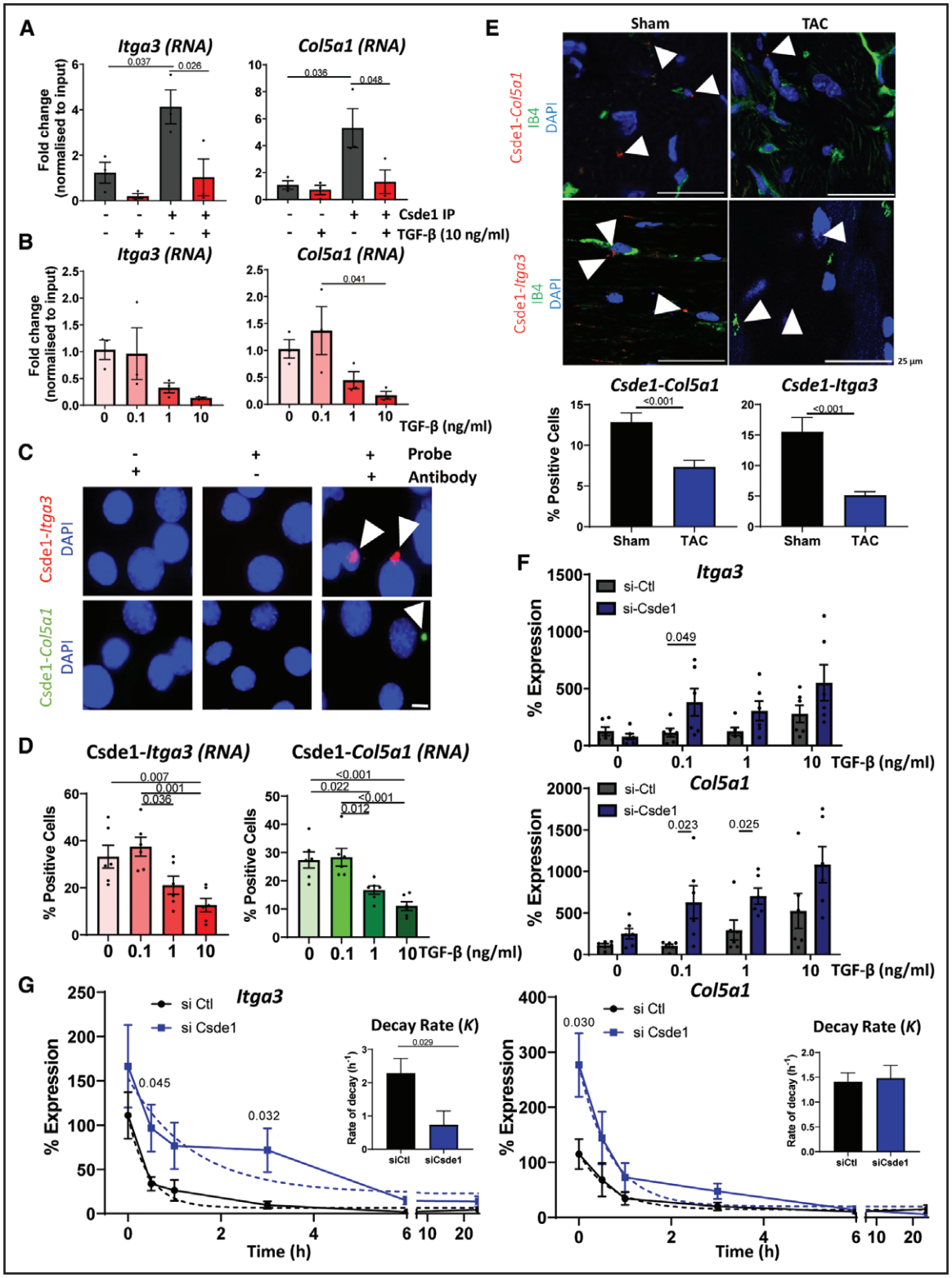

Figure 7. Characterization of the interactions between RNA and Csde1 (cold shock domain containing E1).
A, RNA immunoprecipitation (RIP) Validation of target RNAs. Quantitative polymerase chain reaction (qPCR) analysis of the enrichment of *Itga3* and *Col5a1*RNA in Csde1 immunoprecipitation (IP) samples ± TGF (transforming growth factor)-β stimulation (10 ng/mL, 24 hours) compared with IgG controls. Normalized to input expression. n=3, data shown as average±SEM, normality tested by Shapiro-Wilk test, significance assessed by 1-way ANOVA with Tukey multiple comparison test, significance shown to 3 significant figures. **B**, Effects of TGF-β on target binding. qPCR analysis of *Itga3* and *Col5a1* abundance in Csde1 IPs in the presence of increasing concentrations of TGF-β stimulation (24 hours). Relative to input, n=3, data shown as average±SEM, normality tested by Shapiro-Wilk test, significance assessed by 1-way ANOVA with Tukey multiple comparison test, significance shown to 3 significant figures. **C**, Validation of interactions in situ (*Continued*)

in change in RNA-binding following TGF-β stimulation, revealing several key RBPs (Figure 1F). The changes in RNA-binding abundance of selected RBPs (hnRNP H1, hnRNP F, Csde1, Mov10 [Helicase Mov10], and Eif3C [eukaryotic translation initiation factor 3 subunit C]) were validated by RIC (±ultraviolet crosslinking and TGF-β stimulation) and Western blot analysis, which showed isolation of proteins only after ultraviolet crosslinking and confirmed significant TGF-β driven changes in RBP abundance in RIC isolates (normalized to their abundance in input lysate) for all selected RBPs except Mov10. This suggested that TGF-β stimulation results in increased or decreased interaction between the RBPs and target RNA (Figure 1G and 1H).

RNA-Binding Patterns of TGF-β–Regulated RBPs Correlates With EC Function and Mesenchymal Activation

As TGF-β stimulation resulted in significant changes in the abundance of several key RBPs present in RIC isolates, we investigated the correlation between these changes and the development of EndoMA. Real-time quantitative polymerase chain reaction analysis revealed that TGF-β stimulation resulted in a dose and time-dependent increase in the expression of several key mesenchymal marker genes, while the expression of characteristic EC genes remained largely unchanged in MCECs, suggesting that TGF-β resulted in the activation of a more mesenchymal phenotype without the complete loss of endothelial identity (Figure 2A and 2B). TGF-β stimulation also resulted in drastically inhibited tubule formation (a read-out for endothelial angiogenic function) and widespread changes in RNA expression of genes linked to mesenchymal activation (Figure S2A through S2D).

RIC and subsequent Western blot analysis after incubation in increasing concentrations of TGF-β for 24 hours found significantly increased hnRNP H1 and hnRNP F and significantly decreased Csde1 in RIC isolates in a dose-dependent manner (Figure 2C and 2D). Likewise, RIC and Western blot analysis after incubation with TGF-β for increasing times showed the largest changes in hnRNP H1, hnRNP F, and Csde1 abundance in RIC isolates after 24 hours, correlating with the development of a mesenchymal activation in MCECs (Figure 2B, 2E, and 2F). Interestingly, we found that the expression of the vast majority of TGF-β–regulated RBPs did not change at the RNA or protein level on TGF-β stimulation, including unaltered expression of hnRNP H1, hnRNP F, and Csde1, demonstrating that changes in abundance in RIC isolates reflect a difference in the amount of the RBPs that are bound to RNA rather than changes in their expression (Figures 2C and 2E; Figure S2E).

As TGF-β stimulation impacted the RNA binding of hnRNP H1 and Csde1, we investigated how their localization changed on TGF-β stimulation. MCECs were incubated with increasing concentrations of TGF-β followed by nuclear-cytoplasmic fractionation, showing a significant increase of hnRNP H1 in the nuclear fraction on TGF-β stimulation, without significant alterations in Csde1 localization. Efficient separation of the 2 compartments was demonstrated by Lamin A/C as a nuclear marker and GAPDH as a cytoplasmic marker (Figure 2G and 2H).

To investigate if changes in the RNA binding of hnRNP H1 and Csde1 are downstream of TGF-β receptor signaling, we incubated MCECs with the TGF-β receptor (ALK [anaplastic lymphoma kinase]) inhibitor SB431542 in the presence of TGF-β, followed by RIC and Western blot analysis (Figure 2I). TGF-β receptor inhibition resulted in a significant decrease in the amount of hnRNP H1 that was bound to RNA and an apparent increase in the proportion of RNA-bound Csde1 (not statistically significant). In contrast, inhibition of PI3K (phosphoinositide 3-kinase)/AKT and ERK (extracellular-signal regulated kinase) signaling had no differential effect on RNA binding (Figure S3A and S3B).

Figure 7 Continued. by proximity ligation assay (PLA) assay. PLA assay in mouse cardiac endothelial cells (MCECs) showing the interaction between Csde1 and *Itga3* (red) or *Col5a1* (green) RNA, representative images, scale bar 10 µm. **D**, Effects of TGF-β on Csde1 interactions. Quantifications of changes in Csde1 interaction with *Itga3* or *Col5a1* RNA after stimulation with increasing concentrations of TGF-β (24 hours). Normality tested by Shapiro-Wilk test, significance assessed by 1-way ANOVA with Tukey multiple comparison test, significance shown to 3 significant figures **E**, Validation of interactions in vivo. PLA assay of the interaction of Csde1 with *Itga3* (**top**) or *Col5a1* (**bottom**; interactions red) in mouse heart sections 2 weeks following sham or transverse aortic constriction (TAC) surgery. IB4 (green) shows endothelial cells, nuclei stained with DAPI (blue). Representative images, scale bar 25 µm. Arrowheads point to positive interactions. Graphs show number of interactions normalized to the number of cells per visible field. Error data shown as average±SEM. Normality was assessed by Shapiro-Wilk test, significance was assessed by unpaired Student *t* test, and significance was shown to 3 significant figures. **F**, Effects of Csde1 on Col5a1 and Itga3 expression. qPCR analysis of the changes of expression of *Itga3* and *Col5a1* following TGF-β stimulation and si-Csde1 knockdown. Normalized to *Gapdh*, n=6, data shown as average±SEM, normality was assessed by Shapiro-Wilk test, significance assessed by unpaired Student *t* test between Csde1 and si-control conditions, significance shown to 3 significant figures. **G**, Effects of Csde1 on RNA stability. Csde1 was knocked down with siRNA for 48 hours before the addition of actinomycin D 10 µg/mL to inhibit transcription. RNA abundance was measured by real-time qPCR (normalized to *Gapdh*), and a nonlinear regression curve was calculated to assess effects on RNA stability. n=6, data shown as average±SEM, normality assessed by Shapiro-Wilk, and significance assessed by unpaired Student *t* test between corresponding conditions, significance shown to 3 significant figures. Bar charts show the averaged decay constant, K, ±SEM, of each nonlinear regression curve with significance assessed by unpaired Student *t* test, with significance shown to 3 significant figures. DAPI indicates 4′,6-diamidino-2-phenylindole; IB4, isolectin B4; siCsde1, Csde1 siRNA; siCtl, control siRNA; and siRNA, small interfering RNA.

Next, we investigated if TGF-β driven changes in RNA binding of hnRNP H1 and Csde1 were conserved in other cardiac cell types. Interestingly, we found significant changes in RNA binding of both proteins in NIH/3T3 fibroblast cells (Figure 2J) but not in HL1 cardiomyocytes (Figure 2K). This again suggested that TGF-β impact on the amount of hnRNP H1 and Csde1 that are bound to RNA correlates with mesenchymal gene expression, which is typically induced in fibroblasts and ECs, but less in muscle cells.

TGF-β–Regulated RBPs hnRNP H1 and Csde1 Maintain Endothelial Function and Inhibit Mesenchymal Activation in ECs

Because hnRNP H1 and Csde1 displayed TGF-β–regulated changes in their RNA-binding patterns correlating with increased expression of mesenchymal genes, we investigated their functional impact on this process by siRNA knockdown (Figure 3A and 3B). hnRNP H1 knockdown resulted in increased mesenchymal gene expression, including significantly enhanced fibronectin1 (*Fn1*), α-Smooth muscle actin (*Sma),* SM22-α (*Sm22), TGF-β2*, and *Col1a1* expression. Csde1 knockdown also resulted in significantly increased *Fn1, Sma,* and *Sm22,* as well as significantly increased *Col3a1* and *Col5a1* mRNAs. The expression of EC marker genes (platelet and EC adhesion molecule 1 (*Pecam1*), endothelial nitric oxide synthase [*eNOS*]), however, was not significantly altered. Knockdown of either hnRNP H1 or Csde1 resulted in significantly altered tubule formation in MCECs under basal conditions and the presence of mild TGF-β stimulation, suggesting that these proteins may play a role in facilitating normal angiogenic function in ECs (Figure 3C). Furthermore, knockdown of either protein significantly reduced tubule formation in HUVECs, despite the absence of TGF-β stimulation (Figure S5D). We also observed increased migration, an indicator of a more mesenchymal phenotype, in MCECs after hnRNP H1 knockdown in the absence of TGF-β stimulation and after Csde1 knockdown in the presence of TGF-β stimulation (Figure 3D). Next, we investigated the effects of hnRNP H1 and Csde1 knockdown on LDL uptake (while not a specific endothelial trait, acetylated LDL uptake is considered a marker of normal endothelial function) finding that knockdown of hnRNP H1 and Csde1 both resulted in significantly decreased LDL uptake in the absence of TGF-β stimulation suggesting that both proteins promote normal endothelial function (Figure 3E). Smad 2/3 activation was not changed on downregulation of Csde1 and hnRNP H1, indicating that these proteins do not primarily interfere with canonical TGF-β–dependent signal-transduction (Figure 3F).

Next, we investigated the effect of overexpressing hnRNP H1 and Csde1 in MCECs. Analysis of endothelial and mesenchymal marker gene expression showed that after TGF-β stimulation, hnRNP H1 overexpression resulted in increased expression of *Pecam1* and a significant decrease in *TGF-β2* and *Col1a1* expression (Figure S4A). Csde1 overexpression in TGF-β–stimulated cells led to a significant increase in *eNOS* expression and a significant decrease in *Fn1* and *Col3a1* expression (Figure S4B). Interestingly, overexpression of either protein preserved the tubule-forming ability of MCECs at 0.1 and 1 ng/mL of TGF-β stimulation (Figure S4C), and analysis of LDL uptake showed Csde1 overexpression significantly increased LDL uptake in nonstimulated and TGF-β–stimulated cells, whereas hnRNP H1 overexpression significantly increased LDL uptake in TGF-β–stimulated cells (Figure S4D). These results indicated that overexpression of Csde1 and hnRNP H1 partially inhibited mesenchymal activation and protected EC function during TGF-β stimulation.

To investigate if hnRNP H1 and Csde1 also play a role in regulating the function of human ECs, we validated that TGF-β driven changes in RNA binding are conserved in HCMECs and HUVECs (Figure 3G; Figure S5A). We also validated that hnRNP H1 and Csde1 knockdown resulted in significantly increased mesenchymal gene expression, significantly decreased LDL uptake, and significantly impaired tubule formation in HCMECs and HUVECs (Figure 3H; Figure S5B through S5F).

Identification of hnRNP H1 Target RNAs in ECs

Having found that loss of hnRNP H1 results in mesenchymal activation in ECs, we used RNA immunoprecipitation followed by RNA-seq (RIP-seq) to identify RNAs bound by hnRNP H1 in the presence or absence of TGF-β stimulation (10 ng/mL, 24 hours). Changes in RNA binding were identified after subtraction of matched input samples to account for TGF-β driven changes in RNA abundance (Figure 4A; Table S2). hnRNP H1 bound 1661 RNAs, of which the majority (939) were protein-coding and 59% were bound differentially ($P<0.05$) on TGF-β stimulation (Figure 4B and 4C). Analysis of KEGG pathways among protein-coding targets revealed enrichment of terms linked to not only TGF-β–associated signaling, such as the PI3K-Akt, mTOR (mammalian target of rapamycin), or MAPK, signaling circuits but also focal adhesion and proteoglycan-related RNAs, confirming a potential role in extracellular matrix gene regulation (Figure 4D). In addition, RNAs related to spliceosomes or RNA transport were enriched. Interestingly, proteins involved in RNA metabolism, focal adhesion, and proteoglycans, as well as MAPK and mTOR signaling were further enriched in targets dynamically bound on TGF-β exposure (Figure 4D).

As peaks identified during RIP-sequencing reflect enrichment of the specific parts of the RNA molecules that are bound by hnRNP H1 during immunoprecipitation,

we used this information to gain insight into specific changes in the RNA-binding patterns of hnRNP H1 induced by TGF-β stimulation (Figure 4E and 4F). Mapping the location of these sites within the mRNAs revealed that TGF-β stimulation resulted in a shift in binding more towards the 5' end of the coding region of target RNAs (Figure 4E). We searched for sequence motifs enriched within peaks identified in hnRNP H1 IPs, which suggested that TGF-β stimulation results in a broader RNA-binding pattern by hnRNPH1 compared with nonstimulated conditions (Figure 4F).

To identify the high confidence and most functionally relevant targets of hnRNP H1, we performed RNA-seq from MCECs with and without TGF-β stimulation (10 ng/mL for 24 hours) in the presence or absence of hnRNP H1 knockdown (si-hnRNP H1, 48 hours; Figure 4G; Table S3). Knockdown of hnRNP H1 resulted in distinct changes in RNA expression, including significantly changed expression of 369 RNAs under basal conditions and 375 RNAs after TGF-β stimulation ($P<0.05$; Figure 4G, Table S3). KEGG enrichment analysis showed that in the absence of TGF-β stimulation, hnRNP H1 knockdown resulted in altered expression of RNAs linked to a range of pathways, whereas after TGF-β stimulation, hnRNP H1 knockdown triggered a specific upregulation of genes involved in mesenchymal activation, including TGF-β, PI3K-AKT, HIF-1 (hypoxia-inducible factor 1) signaling, focal adhesion and ECM-receptor interaction (Figure 4H and 4I). We also found distinct changes in alternative splicing patterns following knockdown of hnRNP H1, including enrichment for genes with functions in cell-matrix adhesion (Figure S6). This also revealed an increased alternative 5′ splicing after TGF-β stimulation, correlating with the changes in binding patterns observed in RIP-seq analysis. To assess how differentially expressed genes identified in RNA-seq correlated with the RNAs bound by hnRNP H1 identified in RIP-seq, we overlapped the 2 data sets, revealing 51 RNAs identified as hnRNP H1 binding targets that were also differentially expressed after hnRNP H1 knockdown, and 8 RNAs which were bound by hnRNP H1 and exhibited significantly altered splicing patterns after hnRNP H1 knockdown (Figure 4J). Based on this analysis, we validated the binding of hnRNP H1 to *Smad6* and *Col1a1* RNA by RIP and qPCR analysis (RIP-qPCR), comparing enrichment of these target RNAs between hnRNP H1 IPs in the presence and absence of TGF-β stimulation and matched IgG negative controls (Figure 5A). This revealed significant enrichment of *Smad6* and *Col1a1* RNA in hnRNP H1 pulldowns from TGF-β stimulated cells compared with both basal conditions and IgG controls. Following this, we characterized how binding of hnRNP H1 to *Col1a1* and *Smad6* mRNAs changed in response to increasing doses of TGF-β by RIP-qPCR, showing significantly increased binding with increasing TGF-β when normalized to expression in matched input samples (Figure 5B). By designing biotinylated DNA probes specific to either *Smad6* or *Col1a1* RNA, we used a proximity ligation assay (PLA) to visualize their specific interaction with hnRNP H1 in situ in MCECs. We validated the interaction of hnRNP H1 with *Smad6* and *Col1a1*, finding that these interactions occur almost exclusively in the nucleus (Figure 5C). Increasing concentrations of TGF-β triggered a higher number of cells positive for both hnRNP H1-*Smad6* and hnRNP H1-*Col1a1* interactions after stimulation with 1 and 10 ng/mL TGF-β compared with unstimulated or 0.1 ng/mL TGF-β (Figure 5D). We confirmed the interaction between hnRNP H1 and *Smad6* and *Col1a1* RNA in both healthy (sham operated) and TAC (pathological pressure overload, in which typically EndoMA occurs, Figure S8A) mouse heart sections by PLA, finding that these interactions were present under both conditions but with a higher enrichment of interactions after TAC (Figure 5E). Furthermore, hnRNP H1 expression was upregulated in both whole heart and isolated cardiac ECs following TAC, along with significantly increased Col1a1 expression in whole heart and ECs (Figure S8B).

An important function of RBPs is to regulate RNA abundance and modify RNA stability. This can be achieved either by direct action on the target gene or indirectly through regulating or recruiting other proteins. Thus, we investigated the effects of hnRNP H1 on *Col1a1* and *Smad6* RNA abundance and stability. The knockdown of hnRNP H1 led to reduced abundance of *Smad6* following stimulation with TGF-β (Figure 5F). Under transcriptional inhibition by Actinomycin D, knockdown of hnRNP H1 resulted in decreased *Smad6* RNA abundance, but unchanged *Smad6* half-life, indicating that hnRNP H1 may promote *Smad6* expression by means other than influencing its decay rate (Figure 5G). Knockdown of hnRNP H1 resulted in significantly increased *Col1a1* RNA and increased RNA stability, demonstrated by a decrease in the *Col1a1* decay rate, suggesting hnRNP H1 may suppress *Col1a1* expression by promoting its degradation (Figure 5F and 5G).

Together, EC hnRNP H1 dynamically bound and regulated the expression of RNAs related to PI3K-AKT, HIF-1, and TGF-β signaling and extracellular matrix and thereby off set mesenchymal activation in response to TGF-β stimulation. Smad6, for example, is a canonical inhibitor of TGF-β signaling, suggesting that hnRNP H1 promoted *Smad6* expression following TGF-β stimulation and thereby prevented mesenchymal activation. On the other hand, *Col1a1* RNA abundance was reduced by hnRNP H1 to counteract an important part of the pro-mesenchymal response of ECs to TGF-β stimulation.

Identification of Csde1 Target RNAs in ECs

We used RIP-seq analysis to identify RNAs bound by Csde1 with and without TGF-β stimulation (10 ng/mL

for 24 hours; Figure 6A; Table S4) in MCECs. We identified 2847 bound target RNAs, of which the majority were protein-coding (1821 protein-coding targets) and 58% were bound differentially ($P<0.05$) on stimulation with TGF-β (Figure 6B and 6C). KEGG pathway terms enriched among Csde1 RNA targets were related to functions in, for instance, ubiquitin-mediated proteolysis, cell cycle, tight junctions, proteoglycans, PI3K/AKT, Hippo and MAPK signaling, focal adhesions, and adherens junctions (Figure 6D). Interestingly, all of these terms were further enriched among RNAs bound dynamically by Csde1 on TGF-β stimulation. Analysis of enriched peaks within the mRNA of Csde1 targets found that TGF-β stimulation resulted in specific changes in the binding patterns of Csde1, with a decrease in 3′ untranslated region (UTR) and coding sequence binding and a distinct increase in 5′UTR binding on TGF-β stimulation (Figure 6E). Analysis of enriched motifs revealed strong changes between nonstimulated and TGF-β stimulated conditions, suggesting TGF-β stimulation alters the RNA-binding patterns of Csde1 in a sequence-specific manner (Figure 6F).

RNA-seq showed that knockdown of Csde1 (si-Csde1, 48 hours) in MCECs triggered significant changes in the expression of 259 genes ($P<0.05$) under basal conditions. A much larger number of RNAs (2901, $P<0.05$) were altered in the presence of TGF-β (10 ng/mL), suggesting a prominent role of Csde1 in the regulation of TGF-β–mediated gene expression (Figure 6G; Table S5). Analysis of enriched KEGG pathway terms showed that basal Csde1 knockdown resulted, for example, in the upregulation of genes involved in TGF-β signaling, regulation of stem cell pluripotency, $P<0.05$ were considered statistically significant and proteoglycans. Csde1 knockdown in the presence of TGF-β led to the upregulation of RNAs involved, among others, in stem cell pluripotency regulation, PI3K-AKT signaling, focal adhesion, ECM-receptor interaction, and proteoglycans and an accompanying downregulation of genes involved in p53 signaling and oxidative phosphorylation (Figure 6H and 6I). We also found distinct changes in splicing patterns in many related genes following Csde1 knockdown, with enriched genes involved in cytoskeletal organization and morphogenesis (Figure S7).

Overlapping of RIP-seq and RNA-seq data sets revealed 446 RNAs as binding targets of Csde1 in the RIP-seq analysis that are also differentially expressed on knockdown of Csde1. Four binding targets of Csde1 exhibited differential splicing patterns (Figure 6J). We validated the binding of Csde1 to *Itga3* and *Col5a1* RNA by RIP-qPCR showing a significant enrichment of binding under basal conditions compared with both TGF-β stimulated cells and IgG controls (Figure 7A). We characterized how the binding of Csde1 to these targets changed in response to increasing TGF-β by RIP-qPCR, showing a decrease in affinity to *Col5a1* and *Itga3* with increasing TGF-β (Figure 7B). Using DNA probes specific to *Itga3* and *Col5a1,* we visualized the interaction of Csde1 with these targets in situ in MCECs using PLA, finding that they occur almost exclusively in the cytoplasm, predominantly in the perinuclear area (Figure 7C). We also found a significant decrease in Csde1-*Itga3* and Csde1-*Col5a1* positive cells after 1 ng/mL or 10 ng/mL TGF-β stimulation compared with 0 ng/mL or 0.1 ng/mL TGF-β (Figure 7D). We validated the interaction between Csde1 and *Itga3* and *Col5a1* in ECs in vivo in both sham and TAC hearts, which showed a decrease in these interactions following TAC (Figure 7E). Furthermore, *Csde1* expression was upregulated 2 weeks following TAC (though not statistically significant in ECs), along with significantly increased *Col5a1* and *Itga3* (the latter not statistically significant; Figure S8C).

Analysis of *Itga3* and *Col5a1* abundance following Csde1 knockdown resulted in a significant increase in both *Itga3* and *Col5a1* RNA abundance on different doses of TGF-β (Figure 7F). Mechanistically, Csde1 knockdown significantly increased the stability of *Itga3,* but not of *Col5a1*, following Actinomycin D treatment (Figure 7G). These data suggested that the TGF-β driven decrease in the binding affinity of Csde1 to targets like *Itga3* and *Col5a1* promotes mesenchymal activation in ECs.

DISCUSSION

TGF-β is known as a key driver of mesenchymal activation in ECs, governing the extent to which these cells lose their endothelial and attain more mesenchymal characteristics.[3,4,10,11] The capacity of ECs to transition towards a more mesenchymal phenotype is increasingly emerging as a source of pathological organ fibrosis (eg, see Tombor et al,[8] Froese et al,[9] Zeisberg et al,[26] and Hashimoto et al[27]). Therefore, the ability to specifically modulate the response of ECs to TGF-β stimulation might offer unique opportunities to therapeutically offset the development of pathological fibrosis and maintain or promote endothelial function. Although previous work has provided detailed insights into how TGF-β exerts effects via downstream signaling pathways and transcriptional regulation,[3,10,11,13] mechanisms by which TGF-β acts at the post-transcriptional level have to date been largely neglected.

To address this, we aimed to identify global TGF-β–driven changes in mRNA-binding proteins in a cardiac EC line using RIC. We identified a comparatively small RNA interactome (see screens compiled in Hentze et al[20] for instance) with clear enrichment for known RBPs, of which a large proportion showed TGF-β–regulated changes after stimulation. As TGF-β did not alter the expression of these RBPs, we concluded that these changes predominantly resulted from increased or decreased interactions with their target RNAs. This could be due to either altered RNA-binding activity or

changes in the expression of their target RNAs. Considering our focus to identify the RBPs playing key roles in the post-transcriptional regulation of TGF-β dependent activation of a promesenchymal phenotype (EndoMA), we then focused on the known RBPs that most significantly changed their RNA binding in response to TGF-β.

Two canonical RBPs, Mov10 and Csde1, both known to regulate mRNA stability and translation,[28,29] stood out among RBPs that decreased in RNA binding after TGF-β stimulation. In contrast, 2 members of the hnRNP family of RBPs, hnRNP H1 and hnRNP F, primarily nuclear RBPs best characterized for roles in splicing and RNA processing,[30] emerged as having significantly increased RNA binding in response to TGF-β. Interestingly, the TGF-β driven changes in the RNA-binding patterns of these proteins directly correlated with the onset of a TGF-β–driven increase in mesenchymal gene expression in ECs, suggesting they may play a role in mesenchymal activation. To analyze how RBPs coordinate and fine-tune this process, we then decided to focus on 2 RBPs, hnRNP H1 and Csde1, that exhibited opposing changes in RNA binding on TGF-β stimulation for further characterization.

hnRNP H1 is a ubiquitously expressed member of the hnRNP family.[31] Containing 3 quasi–RNA-recognition motifs, hnRNP H1 primarily functions in splicing and polyadenylation dynamics, although it is known to play different roles in the regulation of RNA metabolism (eg, nuclear export, stability, localization, and translation efficiency).[32,33] Others have shown that hnRNP H1 is involved in the regulation of cell differentiation and vascular signaling.[34–37] Notably, hnRNP H1 also impacts embryonic stem cell differentiation, whereby loss of hnRNP H1 destabilizes ES cell colonies and induces their differentiation.[36] Interestingly, hnRNP H1 acts to repress inflammatory signaling by regulating IL8 (interleukin 8) expression, a proinflammatory cytokine secreted by ECs to regulate vascular permeability.[35–37] Here, we found that the knockdown of hnRNP H1 resulted in increased mesenchymal activation and reduced EC-characteristics. Accordingly, the mRNA targets to which it exerted increased binding on TGF-β stimulation predominantly encoded genes functioning in the regulation of TGF-β signaling as well as extracellular matrix-related genes. For instance, we found that on TGF-β stimulation hnRNP H1 binds with increased affinity to mRNAs encoding for *Smad6*, a canonical antagonist of TGF-β signaling,[38,39] and *Col1a1,* a classical component of the extracellular matrix associated with fibrosis and EndoMA.[40] We observed a TGF-β driven increase in RNA binding, despite no change in hnRNP H1 levels 24 hours of TGF-β stimulation in MCECs, suggesting that TGF-β results in acute and specific changes of RNA-binding regulation, for example, increased RNA-binding activity.

We show that hnRNP H1 differentially acts to increase the expression of *Smad6* while inhibiting *Col1a1* expression, the latter via decreasing its RNA stability. Indeed, other studies have demonstrated the capacity of hnRNP H1 to regulate gene expression at the level of both RNA stability and translation, in addition to its characteristic roles in splicing.[41,42] The effects of hnRNP H1 on the stability of its targets might at least partially result from the TGF-β driven shift in its RNA-binding pattern from the 3′UTR to increased binding of the 5′ end and the gene body. We suggest that the increased amount of RNA-bound hnRNP H1 on TGF-β stimulation acts to offset the development of a mesenchymal phenotype and to protect endothelial function by exerting coordinated and diverse effects on its target RNAs, for example by increasing the expression of the negative TGF-β signaling regulator *Smad6* and by direct inhibition of the expression of matrix genes, such as *Col1a1*. Reassuringly, our RNA-sequencing data supported our hypothesis, confirming upregulation of promesenchymal and EndoMA related pathways after hnRNP H1 knock down.

Csde1 is a well-characterized RBP mainly localized in the cytoplasm.[43] It contains 5 cold shock domains and performs a range of functions governing mRNA translation dynamics and stability, interacting with various complexes and targets in a cell type and state-dependent manner to increase or decrease the translation or stability of specific subsets of its targets.[29,44] Previous studies have shown that Csde1 plays a role in embryonic stem cell differentiation and the differentiation of the primitive endoderm.[45,46] Csde1 is also known to act as both a promoter and suppressor of oncogenesis in a context-dependent manner and has been shown to directly interact with TGF-β1 RNA and other related RNAs in cancer cells to influence metastasis and migration.[29,47,48]

Previous data showed that Csde1 preferentially binds to the 5′ UTR of selective RNA targets, allowing it to impact early translational elongation.[47] We confirmed increased 5′UTR binding for endothelial Csde1 specifically on TGF-β stimulation, although we did not further investigate this mode of action in our study. Intriguingly, in the case of melanoma and colorectal cancer, Csde1 plays an important role in regulating cytoskeletal and extracellular matrix components to promote migration and metastasis by enhancing the expression of pro-metastatic genes such as vimentin, while inhibiting the expression of other mesenchymal genes like fibronectin 1.[46,49] We found that Csde1 overexpression protects key endothelial phenotypic characteristics and inhibits EndoMA, whereas knockdown of Csde1 promotes mesenchymal activation. Again, this was reflected by our RNA-sequencing data. As an example, we showed that Csde1 knockdown resulted in increased expression of *Itga3* and *Col5a1*, 2 promesenchymal targets known to be upregulated by TGF-β.[50,51] Both targets exhibited reduced interaction with Csde1 on TGF-β stimulation

leading to increased expression, suggesting that binding of Csde1 diminishes the stability of their mRNAs.

Together, our data suggests that Csde1 and hnRNP H1 both play important roles in counteracting mesenchymal activation in ECs. In response to TGF-β as well as TAC, however, their binding to DNA is differentially regulated. On one hand, TGF-β or TAC stimulation drives reduced Csde1 binding to mRNA, which in turn facilitates EndoMA in a feed-forward loop. On the other hand, the increase in hnRNP H1 binding induced by TGF-β or TAC offsets this, acting as a brake on promesenchymal progression and preventing the complete loss of EC function (perhaps facilitating a transient mesenchymal phenotype and preventing a complete loss of endothelial characteristics) in a negative feedback. Our findings suggest a complex post-transcriptional RBP system to respond to growth factors like TGF-β and coordinate a balanced cellular response. Given that modulating EndoMA or endothelial-to-mesenchymal transition is emerging as a potential target for therapeutic intervention to prevent pathological fibrosis, the ability to exploit the RNA-binding dynamics of hnRNP H1 or Csde1 may offer invaluable opportunities in the future. Further work should be performed to characterize the importance of hnRNP H1 and Csde1 in ECs in health and disease in mouse models in vivo as well as to examine the therapeutic potential to modulate their interactions with RNA.

LIMITATIONS

This study investigated the role of RBPs as regulators of TGF-β signaling at the post-transcriptional level in a mouse cardiac EC line, with a specific focus on the context of mesenchymal activation (EndoMA), but key findings were confirmed in human primary ECs. TGF-β signaling prompts a range of cellular responses in a cell type and context-dependent manner, including within ECs.[52] It would, therefore, be of further interest to analyze the functions of these TGF-β–regulated RBPs in different cell types and context, to examine if their functions are specific to the regulation of EC function and EndoMA.

Furthermore, we have identified these proteins as regulators of the response to TGF-β, of EC function, and the development of EndoMA predominantly in an in vitro setting. This has enabled us to screen for and identify candidates that we think are likely to play a physiological role in modulating endothelial response to TGF-β stimulation and the development of EndoMA in vivo. However, the physiological setting in vivo is naturally more complex, and although we validated that specific interactions occurred differentially in heart sections from a cohort of male mice following TAC, further studies are required to characterize the role and importance of these RBPs in vivo, including in cohorts of female mice.

ARTICLE INFORMATION

Received July 26, 2023; accepted August 18, 2023.

Affiliations

Department of Cardiovascular Physiology (R.W., M.K., I.P., S.H., S.G., J.H.), Cardiovascular Pharmacology (R.O.), and Cardiovascular Genomics and Epigenomics (G.D.), European Center for Angioscience (ECAS), Medical Faculty Mannheim of Heidelberg University, Germany. German Center for Cardiovascular Research (DZHK), partner site Heidelberg/Mannheim (R.W., M.K., S.H., S.G., G.D., J.H.). Proteomics Core Facility, European Molecular Biology Laboratory (EMBL), Heidelberg, Germany (J.S., F.S.). European Molecular Biology Laboratory (EMBL), Heidelberg, Germany (M.W.H.).

Acknowledgments

The authors would like to thank members of the Hentze group for experimental advice (proximity ligation assay). The authors also thank the Live Cell Imaging Facility in Mannheim (LIMA) for their support with confocal microscopy and the Proteomics Core Facility (European Molecular Biology Laboratory) for support with proteomic analysis. R. Wardman, I. Pachkiv, M. Keles, S. Hemanna, and S. Grein conducted experiments and analyzed data. J. Schwarz and F. Stein conducted the proteomic analysis. R. Ola, G. Dobreva, and M.W. Hentze provided advice, reagents, and methodological concepts for the study. J. Heineke conceptualized the study. R. Wardman and J. Heineke designed experiments and prepared the article. JH supervised the study and all experimentation.

Sources of Funding

J. Heineke was supported by the SFB1366/1-A6 (J. Heineke) from the Deutsche Forschungsgemeinschaft and the DZHK (Deutsches Zentrum für Herz-Kreislauf-Forschung - German Center for Cardiovascular Research) and the BMBF (German Ministry of Education and Research).

Disclosures

None.

Supplemental Material

Figures S1–S8
Tables S1–5
Western Blot Source Data
Major Resources Table

REFERENCES

1. Augustin HG, Koh GY. Organotypic vasculature: from descriptive heterogeneity to functional pathophysiology. *Science*. 2017;357:eaal2379. doi: 10.1126/science.aal2379
2. Aird WC. Endothelial cell heterogeneity. *Cold Spring Harb Perspect Med*. 2012;2:a006429. doi: 10.1101/cshperspect.a006429
3. Kovacic JC, Dimmeler S, Harvey RP, Finkel T, Aikawa E, Krenning G, Baker AH. Endothelial to mesenchymal transition in cardiovascular disease: JACC state-of-the-art review. *J Am Coll Cardiol*. 2019;73:190–209. doi: 10.1016/j.jacc.2018.09.089
4. Pardali E, Sanchez-Duffhues G, Gomez-Puerto MC, Ten Dijke P. TGF-β-induced endothelial-mesenchymal transition in fibrotic diseases. *Int J Mol Sci*. 2017;18:2157. doi: 10.3390/ijms18102157
5. Gong H, Lyu X, Wang Q, Hu M, Zhang X. Endothelial to mesenchymal transition in the cardiovascular system. *Life Sci*. 2017;184:95–102. doi: 10.1016/j.lfs.2017.07.014
6. Manavski Y, Abel T, Hu J, Kleinlützum D, Buchholz CJ, Belz C, Augustin HG, Boon RA, Dimmeler S. Endothelial transcription factor KLF2 negatively regulates liver regeneration via induction of activin A. *Proc Natl Acad Sci U S A*. 2017;114:3993–3998. doi: 10.1073/pnas.1613392114
7. Sánchez-Duffhues G, García de Vinuesa A, Ten Dijke P. Endothelial-to-mesenchymal transition in cardiovascular diseases: developmental signaling pathways gone awry. *Dev Dyn*. 2018;247:492–508. doi: 10.1002/dvdy.24589
8. Tombor LS, John D, Glaser SF, Luxán G, Forte E, Furtado M, Rosenthal N, Baumgarten N, Schulz MH, Wittig J, et al. Single cell sequencing reveals endothelial plasticity with transient mesenchymal activation after myocardial infarction. *Nat Commun*. 2021;12:681. doi: 10.1038/s41467-021-20905-1
9. Froese N, Cordero J, Abouissa A, Trogisch FA, Grein S, Szaroszyk M, Wang Y, Gigina A, Korf-Klingebiel M, Bosnjak B, et al. Analysis of myocardial cellular gene expression during pressure overload reveals matrix based functional intercellular communication. *iScience*. 2022;25:103965. doi: 10.1016/j.isci.2022.103965

10. Goumans MJ, Liu Z, ten Dijke P. TGF-beta signaling in vascular biology and dysfunction. *Cell Res*. 2009;19:116–127. doi: 10.1038/cr.2008.326
11. Cooley BC, Nevado J, Mellad J, Yang D, St. Hilaire C, Negro A, Fang F, Chen G, San H, Walts AD, et al. TGF-β signaling mediates endothelial-to-mesenchymal transition (EndMT) during vein graft remodeling. *Sci Transl Med*. 2014;6:227ra34. doi: 10.1126/scitranslmed.3006927
12. Derynck R, Zhang YE. Smad-dependent and Smad-independent pathways in TGF-beta family signalling. *Nature*. 2003;425:577–584. doi: 10.1038/nature02006
13. van Meeteren LA, ten Dijke P. Regulation of endothelial cell plasticity by TGF-β. *Cell Tissue Res*. 2012;347:177–186. doi: 10.1007/s00441-011-1222-6
14. Dreyfuss G, Kim VN, Kataoka N. Messenger-RNA-binding proteins and the messages they carry. *Nat Rev Mol Cell Biol*. 2002;3:195–205. doi: 10.1038/nrm760
15. Mitchell SF, Parker R. Principles and properties of eukaryotic mRNPs. *Mol Cell*. 2014;54:547–558. doi: 10.1016/j.molcel.2014.04.033
16. Xin H, Deng K, Fu M. Post-transcriptional gene regulation by RNA-binding proteins in vascular endothelial dysfunction. *Sci China Life Sci*. 2014;57:836–844. doi: 10.1007/s11427-014-4703-5
17. Fu X, Zhai S, Yuan J. Endothelial HuR deletion reduces the expression of proatherogenic molecules and attenuates atherosclerosis. *Int Immunopharmacol*. 2018;65:248–255. doi: 10.1016/j.intimp.2018.09.023
18. Baltz AG, Munschauer M, Schwanhäusser B, Vasile A, Murakawa Y, Schueler M, Youngs N, Penfold-Brown D, Drew K, Milek M, et al. The mRNA-bound proteome and its global occupancy profile on protein-coding transcripts. *Mol Cell*. 2012;46:674–690. doi: 10.1016/j.molcel.2012.05.021
19. Castello A, Fischer B, Eichelbaum K, Horos R, Beckmann BM, Strein C, Davey NE, Humphreys DT, Preiss T, Steinmetz LM, et al. Insights into RNA biology from an atlas of mammalian mRNA-binding proteins. *Cell*. 2012;149:1393–1406. doi: 10.1016/j.cell.2012.04.031
20. Hentze MW, Castello A, Schwarzl T, Preiss T. A brave new world of RNA-binding proteins. *Nat Rev Mol Cell Biol*. 2018;19:327–341. doi: 10.1038/nrm.2017.130
21. Appari M, Breitbart A, Brandes F, Szaroszyk M, Froese N, Korf-Klingebiel M, Mohammadi MM, Grund A, Scharf GM, Wang H, et al. C1q-TNF-related protein-9 promotes cardiac hypertrophy and failure. *Circ Res*. 2017;120:66–77. doi: 10.1161/CIRCRESAHA.116.309398
22. Castello A, Horos R, Strein C, Fischer B, Eichelbaum K, Steinmetz LM, Krijgsveld J, Hentze MW. System-wide identification of RNA-binding proteins by interactome capture. *Nat Protoc*. 2013;8:491–500. doi: 10.1038/nprot.2013.020
23. Hughes CS, Foehr S, Garfield DA, Furlong EE, Steinmetz LM, Krijgsveld J. Ultrasensitive proteome analysis using paramagnetic bead technology. *Mol Syst Biol*. 2014;10:757. doi: 10.15252/msb.20145625
24. Suzuki K, Bose P, Leong-Quong RY, Fujita DJ, Riabowol K. REAP: a two minute cell fractionation method. *BMC Res Notes*. 2010;3:294. doi: 10.1186/1756-0500-3-294
25. Gagliardi M, Matarazzo MR. RIP: RNA immunoprecipitation. *Methods Mol Biol*. 2016;1480:73–86. doi: 10.1007/978-1-4939-6380-5_7
26. Zeisberg EM, Potenta SE, Sugimoto H, Zeisberg M, Kalluri R. Fibroblasts in kidney fibrosis emerge via endothelial-to-mesenchymal transition. *J Am Soc Nephrol*. 2008;19:2282–2287. doi: 10.1681/ASN.2008050513
27. Hashimoto N, Phan SH, Imaizumi K, Matsuo M, Nakashima H, Kawabe T, Shimokata K, Hasegawa Y. Endothelial-mesenchymal transition in bleomycin-induced pulmonary fibrosis. *Am J Respir Cell Mol Biol*. 2010;43:161–172. doi: 10.1165/rcmb.2009-0031OC
28. Nawaz A, Shilikbay T, Skariah G, Ceman S. Unwinding the roles of RNA helicase MOV10. *Wiley Interdiscip Rev RNA*. 2022;13:e1682. doi: 10.1002/wrna.1682
29. Guo AX, Cui JJ, Wang LY, Yin J-Y. The role of CSDE1 in translational reprogramming and human diseases. *Cell Commun Signal*. 2020;18:14. doi: 10.1186/s12964-019-0496-2
30. Geuens T, Bouhy D, Timmerman V. The hnRNP family: insights into their role in health and disease. *Hum Genet*. 2016;135:851–867. doi: 10.1007/s00439-016-1683-5
31. Ruan QT, Yazdani N, Beierle JA, Hixson KM, Hokenson KE, Apicco DJ, Luttik KP, Zheng K, Maziuk BF, Ash PEA, et al. Changes in neuronal immunofluorescence in the C- versus N-terminal domains of hnRNP H following D1 dopamine receptor activation. *Neurosci Lett*. 2018;684:109–114. doi: 10.1016/j.neulet.2018.07.015
32. Van Dusen CM, Yee L, McNally LM, McNally MT. A glycine-rich domain of hnRNP H/F promotes nucleocytoplasmic shuttling and nuclear import through an interaction with transportin 1. *Mol Cell Biol*. 2010;30:2552–2562. doi: 10.1128/MCB.00230-09
33. Sun YL, Liu F, Liu F, Zhao XH. Protein and gene expression characteristics of heterogeneous nuclear ribonucleoprotein H1 in esophageal squamous cell carcinoma. *World J Gastroenterol*. 2016;22:7322–7331. doi: 10.3748/wjg.v22.i32.7322
34. Lefave CV, Squatrito M, Vorlova S, Rocco GL, Brennan CW, Holland EC, Pan Y-X, Cartegni L. Splicing factor hnRNPH drives an oncogenic splicing switch in gliomas. *EMBO J*. 2011;30:4084–4097. doi: 10.1038/emboj.2011.259
35. Yu H, Huang X, Ma Y, Gao M, Wang O, Gao T, Shen Y, Liu X. Interleukin-8 regulates endothelial permeability by down-regulation of tight junction but not dependent on integrins induced focal adhesions. *Int J Biol Sci*. 2013;9:966–979. doi: 10.7150/ijbs.6996
36. Yamazaki T, Liu L, Lazarev D, Al-Zain A, Fomin V, Yeung PL, Chambers SM, Lu C-W, Studer L, Manley JL. TCF3 alternative splicing controlled by hnRNP H/F regulates E-cadherin expression and hESC pluripotency. *Genes Dev*. 2018;32:1161–1174. doi: 10.1101/gad.316984.118
37. Tanu T, Taniue K, Imamura K, Onoguchi-Mizutani R, Han H, Jensen TH, Akimitsu N. hnRNPH1-MTR4 complex-mediated regulation of NEAT1v2 stability is critical for IL8 expression. *RNA Biol*. 2021;18:537–547. doi: 10.1080/15476286.2021.1971439
38. Imamura T, Takase M, Nishihara A, Oeda E, Hanai J, Kawabata M, Miyazono K. Smad6 inhibits signalling by the TGF-beta superfamily. *Nature*. 1997;389:622–626. doi: 10.1038/39355
39. Miyazawa K, Miyazono K. Regulation of TGF-β family signaling by inhibitory smads. *Cold Spring Harb Perspect Biol*. 2017;9:a022095. doi: 10.1101/cshperspect.a022095
40. Piera-Velazquez S, Li Z, Jimenez SA. Role of endothelial-mesenchymal transition (EndoMT) in the pathogenesis of fibrotic disorders. *Am J Pathol*. 2011;179:1074–1080. doi: 10.1016/j.ajpath.2011.06.001
41. Uren PJ, Bahrami-Samani E, de Araujo PR, Vogel C, Qiao M, Burns SC, Smith AD, Penalva LOF. High-throughput analyses of hnRNP H1 dissects its multi-functional aspect. *RNA Biol*. 2016;13:400–411. doi: 10.1080/15476286.2015.1138030
42. Khan MI, Zhang J, Liu Q. HnRNP F and hnRNP H1 regulate mRNA stability of amyloid precursor protein. *Neuroreport*. 2021;32:824–832. doi: 10.1097/WNR.0000000000001662
43. Dormoy-Raclet V, Markovits J, Malato Y, Huet S, Lagarde P, Montaudon D, Jacquemin-Sablon A, Jacquemin-Sablon H. Unr, a cytoplasmic RNA-binding protein with cold-shock domains, is involved in control of apoptosis in ES and HuH7 cells. *Oncogene*. 2007;26:2595–2605. doi: 10.1038/sj.onc.1210068
44. Mihailovich M, Militti C, Gabaldón T, Gebauer F. Eukaryotic cold shock domain proteins: highly versatile regulators of gene expression. *Bioessays*. 2010;32:109–118. doi: 10.1002/bies.200900122
45. Elatmani H, Dormoy-Raclet V, Dubus P, Dautry F, Chazaud C, Jacquemin-Sablon H. The RNA-binding protein Unr prevents mouse embryonic stem cells differentiation toward the primitive endoderm lineage. *Stem Cells*. 2011;29:1504–1516. doi: 10.1002/stem.712
46. Ju Lee H, Bartsch D, Xiao C, Guerrero S, Ahuja G, Schindler C, Moresco JJ, Yates JR, Gebauer F, Bazzi H, et al. A post-transcriptional program coordinated by CSDE1 prevents intrinsic neural differentiation of human embryonic stem cells. *Nat Commun*. 2017;8:1456. doi: 10.1038/s41467-017-01744-5
47. Wurth L, Papasaikas P, Olmeda D, Bley N, Calvo GT, Guerrero S, Cerezo-Wallis D, Martinez-Useros J, García-Fernández M, Hüttelmaier S, et al. UNR/CSDE1 drives a post-transcriptional program to promote melanoma invasion and metastasis. *Cancer Cell*. 2016;30:694–707. doi: 10.1016/j.ccell.2016.10.004
48. Avolio R, Inglés-Ferrándiz M, Ciocia A, Coll O, Bonnin S, Guitart T, Ribó A, Gebauer F. Coordinated post-transcriptional control of oncogene-induced senescence by UNR/CSDE1. *Cell Rep*. 2022;38:110211. doi: 10.1016/j.celrep.2021.110211
49. Martinez-Useros J, Garcia-Carbonero N, Li W, Fernandez-Aceñero MJ, Cristobal I, Rincon R, Rodriguez-Remirez M, Borrero-Palacios A, Garcia-Foncillas J. UNR/CSDE1 expression is critical to maintain invasive phenotype of colorectal cancer through Regulation of c-MYC and epithelial-to-mesenchymal transition. *J Clin Med*. 2019;8:560. doi: 10.3390/jcm8040560
50. Kahai S, Vary CP, Gao Y, Seth A. Collagen, type V, alpha1 (COL5A1) is regulated by TGF-beta in osteoblasts. *Matrix Biol*. 2004;23:445–455. doi: 10.1016/j.matbio.2004.09.004
51. Zhang H, Cui X, Cao A, Li X, Li L. ITGA3 interacts with VASP to regulate stemness and epithelial-mesenchymal transition of breast cancer cells. *Gene*. 2020;734:144396. doi: 10.1016/j.gene.2020.144396
52. Chen P-Y, Qin L, Li G, Wang Z, Dahlman JE, Malagon-Lopez J, Gujja S, Cilfone NA, Kauffman KJ, Sun L, et al. Endothelial TGF-β signalling drives vascular inflammation and atherosclerosis. *Nat Metab*. 2019;1:912–926. doi: 10.1038/s42255-019-0102-3